Dnmt3bas coordinates transcriptional induction and alternative exon inclusion to promote catalytically active Dnmt3b expression

Mohd Saleem Dar[1], Isaiah K Mensah[1], Ming He[1], Sarah McGovern[1], Mark C Hall[1,2], Hannah Christian Whitlock[1], Nina Elise Bippus[1], Madison Ceminsky[1], Martin L Emerson[1], Hern J Tan[1], Humaira Gowher[1,2*]

[1]Department of Biochemistry; [2]Purdue University Center for Cancer Research; Purdue University; West Lafayette, Indiana 47907 USA

*Correspondence: hgowher@purdue.edu

Running title: Role of *Dnmt3bas* in *Dnmt3b* expression

Summary

During mammalian embryogenesis, DNMT3B activity is critical for the genome-wide establishment of DNA methylation. Using naïve ESC differentiation as a model, we elucidated the mechanism by which lncRNA, *Dnmt3bas,* controls the inducible expression and alternative splicing of *Dnmt3b*. Our data showed that *Dnmt3bas* knockdown increased transcriptional induction and decreased H3K27me3 at Dnmt3b cis-regulatory elements post-differentiation. Notably, transcriptional induction of *Dnmt3b* was accompanied by exon inclusion, switching the major isoform from catalytically inactive *Dnmt3b6* to the active *Dnmt3b1*. While *Dnmt3bas* overexpression attenuated *Dnmt3b* induction, it increased the *Dnmt3b1:Dnmt3b6* ratio. This observation was explained by a specific interaction of *Dnmt3bas* with hnRNPL, which promotes exon inclusion. These data suggest that *Dnmt3bas* coordinates alternative splicing and transcriptional induction of Dnmt3b by facilitating the interaction of hnRNPL and RNA Pol II at the Dnmt3b promoter. This two-pronged mechanism would tightly control DNMT3B activity, ensuring the fidelity and specificity of *de novo* DNA methylation during development.

Introduction

During mammalian development, epigenetic reprogramming, which involves global erasure and re-establishment of DNA methylation, facilitates the acquisition of epigenetic plasticity and limits the inheritance of acquired epimutations (Greenberg and Bourc'his, 2019). DNA methylation is reset by the *de novo* methylation activity of DNMT3A and DNMT3B DNA methyltransferases. In mice, homozygous knockout of *dnmt3a* and *dnmt3b* is embryonic lethal, demonstrating their essential role in mammalian development (Okano et al., 1999; Okano et al., 1998) .

Dnmt3b is dynamically expressed during development, with the highest expression in the early stages. *Dnmt3b*$^{-/-}$ ESC (murine embryonic stem cells) show defective differentiation potential and loss of DNA methylation at the regulatory elements of lineage-specific genes and minor satellite repeats, which are the preferred targets of the *Dnmt3b* enzyme (Gopalakrishnan et al.,

36 2009; Norvil et al., 2020; Okano et al., 1999). In somatic cells, the expression of *Dnmt3b* is low
37 and is controlled in a tissue-specific manner (Robertson et al., 2000; Robertson et al., 1999).
38 *Dnmt3b* is transcribed in more than 30 alternatively spliced isoforms, although only a few have
39 been detected at the protein level (Ostler et al., 2007; Xie et al., 1999). Several of these
40 isoforms are catalytically inactive due to the loss of key catalytic residues. The two major
41 isoforms expressed in normal cells are *Dnmt3b1* and *Dnmt3b6*. The exclusion of exons 22 and
42 23 results in the loss of a significant part of the target recognition region in the Dnmt3b6
43 transcript, thus rendering the protein enzymatically inactive. However, DNMT3B6 has been
44 shown to interact and allosterically activate the full-length catalytically active enzyme DNMT3B1
45 (Duymich et al., 2016; Ostler et al., 2007; Saito et al., 2002; Wang et al., 2007; Weisenberger et
46 al., 2004; Zeng et al., 2020).

47 The aberrant increase in *DNMT3B* expression leads to DNA hypermethylation and loss of gene
48 regulation in various human diseases (Esteller, 2005; Walton et al., 2014; Watanabe and
49 Maekawa, 2010). Sequence polymorphisms in the *DNMT3B* promoter that increase promoter
50 activity are associated with an increased risk of several cancers (Montgomery et al., 2004; Shen
51 et al., 2002; Singal et al., 2005). Loss of function mutations in human *DNMT3B* are highly
52 prevalent in patients with ICF (immunodeficiency, centromeric instabilities, and facial
53 abnormalities) syndrome and cause hypomethylation of repetitive elements and genomic
54 instability in B cells (Gowher and Jeltsch, 2002; Okano et al., 1999; Xie et al., 2006; Xu et al.,
55 1999). Aberrant expression and splicing of *DNMT3B* are linked to the loss of methylation at
56 oncogenes and repetitive elements in diverse cancers, including colorectal, lung, and breast
57 cancers (Guil and Esteller, 2009; Kulis and Esteller, 2010; Mensah et al., 2021; Szyf, 2005).
58 These observations indicate that the highly regulated spatiotemporal expression and alternative
59 splicing of *DNMT3B* are critical for cell differentiation, homeostasis, and survival (Huntriss et al.,
60 2004; Okano et al., 1998). Despite the breadth of evidence supporting the critical role of

61 *DNMT3B* in differentiation and cell identity, little is known about the mechanisms that control its
62 transcription.

63 The murine *Dnmt3b* gene locus comprises a CpG island promoter and an enhancer element ~8
64 kb upstream of the *Dnmt3b* promoter (Ishida et al., 2003; Jinawath et al., 2005). A divergently
65 expressed antisense transcript (*Dnmt3bas*) initiates 1 kb downstream of the *Dnmt3b* promoter
66 and is potentially a long non-coding RNA (lncRNA). LncRNAs have critical cellular functions,
67 including transcription, splicing, translation, RNA export, chromatin looping, and DNA repair.
68 Most lncRNAs are transcribed by RNA Pol II but at lower levels, and many undergo capping,
69 splicing, and polyadenylation (Mele et al., 2017; Statello et al., 2021; Zuckerman and Ulitsky,
70 2019). LncRNAs interact with chromatin proteins and regulate the activation and silencing of
71 genes (Derrien et al., 2012; Guo et al., 2020; Guttman et al., 2009; Guttman et al., 2011; Tian
72 and Manley, 2017). During ESC differentiation, several lncRNAs originate from the divergent
73 transcription. These lncRNA/mRNA gene pairs are coordinately regulated and required for
74 pluripotency and differentiation (Guttman et al., 2011; Luo et al., 2016). Here we report
75 *Dnmt3bas/Dnmt3b* as a coordinately expressed gene pair where the lncRNA*, Dnmt3bas,*
76 regulates transcriptional induction and alternative splicing of *Dnmt3b* mRNA.

77 During differentiation of naive pluripotent mouse embryonic stem cells (2i-ESCs), the temporal
78 expression pattern of *Dnmt3b* is similar to that observed during embryonic development (Ficz et
79 al., 2013; Leitch et al., 2013; Ying et al., 2008), making them an ideal model system. Here we
80 show that in undifferentiated 2i-ESCs, *Dnmt3b* is expressed at a low basal level and primarily as
81 *Dnmt3b6*, the catalytically inactive isoform. The expression of Dnmt3b is strongly induced in
82 response to the differentiation signal and is, interestingly, accompanied by exon inclusion, which
83 promotes the expression of the catalytically active, *Dnmt3b1* as the major isoform. As
84 differentiation proceeds, *Dnmt3b* expression is downregulated. Our study is the first to report the
85 role and mechanism of *Dnmt3bas* in regulating *Dnmt3b* expression and alternative splicing.

Gene expression analysis of undifferentiated 2iESCs and cells post differentiation showed a coordinated yet contrasting expression pattern of *Dnmt3b* and *Dnmt3bas*, with the *Dnmt3b* pattern mimicking the expression of *Dnmt3b* observed *in vivo*. The chromatin modification state of proximal and distal enhancers and enhancer-promoter looping complemented the *Dnmt3b* transcriptional state. Whereas we observed no discernable effect of the downregulation (KD) or overexpression (OE) of *Dnmt3bas* on *Dnmt3b* basal expression, the transcriptional induction of *Dnmt3b* was decreased in *Dnmt3bas* OE cells and increased in *Dnmt3bas* KD cells. Interestingly, the undifferentiated OE cells showed an increase in H3K27me3 at the cis-regulatory elements, suggesting the role of *Dnmt3bas* in regulating PRC2 activity at these sites. Additionally, higher enrichment of H3K27Ac and an increased interaction frequency between enhancer and promoter were observed in the KD cells post-differentiation. In *Dnmt3bas* OE cells, we also observed increased exon inclusion, resulting in higher *Dnmt3b1:Dnmt3b6* ratio. Our systematic experimental analysis determined the splicing factor, hnRNPL, as the binding partner of *Dnmt3bas* that facilitates exon inclusion during transcriptional induction of *Dnmt3b*.

Overall, this comprehensive study elucidated a mechanism by which a promoter-associated lncRNA, *Dnmt3bas*, coordinates transcriptional induction and alternative splicing of an essential developmental gene and establishes the role of cis-regulatory elements in this process.

Keywords: lncRNA, alternative splicing, DNA methylation, chromatin-modifications, promoters, enhancers, Dnmt3b, *Dnmt3bas*

Results

Transcriptional induction and alternative splicing of Dnmt3b

We adapted serum-cultured murine embryonic stem cells (s-ESCs) to 2i media (2i-ESCs). As reported earlier, naïve pluripotency markers were upregulated during the adaptation process. Moreover, the expression of *Dnmt3a* and *Dnmt3b* were downregulated, with the concomitant loss of DNA methylation genome-wide (Figure S1A-1C). We differentiated 2i-ESCs and collected

111 samples from D1-D6 post-differentiation (Fig S1D). Differentiation was monitored by a change in
112 the expression of pluripotency and differentiation markers by RT-qPCR (Fig S1E). Analysis of
113 *Dnmt3b* expression showed a 10-15 fold increase, which peaks at D3, followed by a substantial
114 decrease that stays steady from D4 to D6 post-differentiation (Figure 1A). Since *Dnmt3b* is
115 expressed at a low basal level in 2i-ESCs, the induction is significantly higher than observed
116 during the differentiation of s-ESCs (Figure S1F), making 2i-ESC differentiation an ideal
117 experimental model system.

118 *Dnmt3b* transcripts comprise two major alternatively spliced isoforms, *Dnmt3b1*, a full-length
119 transcript, and *Dnmt3b6*, in which exons 22 and 23 are excluded (Figure 1B). Whereas *Dnmt3b1*
120 codes for an active DNA methyltransferase enzyme, the *Dnmt3b6* protein is inactive due to the
121 absence of motifs critical for catalytic activity (Duymich et al., 2016; Ostler et al., 2007; Saito et
122 al., 2002; Wang et al., 2007; Weisenberger et al., 2004; Zeng et al., 2020). RT-PCR was used to
123 amplify both isoforms pre- and post-differentiation of ESCs (Figure 1B). As shown previously
124 (Gowher et al., 2008), both isoforms are expressed equally in FBS-cultured ESCs. Interestingly,
125 in 2i-cultured ESC, *Dnmt3b* mainly comprises the shorter isoform *Dnmt3b6*, indicating that exon
126 exclusion is preferred during basal transcription of *Dnmt3b*. However, upon differentiation, as
127 *Dnmt3b* expression is induced, *Dnmt3b1* is expressed as the major isoform indicating that the
128 alternative splicing switches in favor of exon inclusion during transcriptional induction Post-
129 differentiation transcriptional repression is again accompanied by switching to exon exclusion,
130 and *Dnmt3b6* is expressed as a major isoform in embryoid bodies (Figure 1B, S1G). These data
131 suggest that in conjunction with transcriptional induction, the alternative exon inclusion/exclusion
132 regulates the level of catalytically active DNMT3B, underscoring the critical role of the alternative
133 splicing.

134 The cis-regulatory elements in the Dnmt3b locus constitute a CpG island promoter and putative
135 proximal and distal enhancer elements located about 0.3 and 8 kilobases upstream of the

136 transcription start site (TSS), respectively (Figure S1H) (ENCODE CRE) (Ficz et al.). To
137 determine the engagement of the putative distal enhancer in the regulation of *Dnmt3b* expression,
138 we examined the enhancer-promoter (E-P) looping interaction pre- and post-differentiation in 2i-
139 ESCs, using a chromatin conformation capture (3C) assay (Hagege et al., 2007; Naumova et al.,
140 2012). We observed a potent and specific contact between the distal enhancer and promoter
141 regions. The E-P loop was prevalent in the undifferentiated 2i-ESC when *Dnmt3b* was expressed
142 at the basal level. However, a significant increase in the interaction frequency was observed on
143 D3 post-differentiation. These observations suggest that pre-positioning the enhancer next to the
144 promoter enables a quick transcriptional response to the induction signal (Figure 1C).

145 Based on the transcriptional state of the associated gene, enhancer regions acquire different
146 chromatin modifications. We measured the enrichment of H3K4me1, H3K27Ac, and H3K27me3
147 at *Dnmt3b* regulatory regions pre- and post-differentiation. At D3 post-differentiation, we observed
148 an expected increase in H3K4me1 and H3K27Ac concomitant with enhancer activation and
149 induction of *Dnmt3b* expression. *Dnmt3b* repression at D6 post-differentiation was associated
150 with a decrease in H3K4me1 and H3K27Ac at both proximal and distal enhancer regions (Figures
151 1D and 1E). In contrast, H3K27me3 at the proximal and distal enhancer regions was higher in
152 undifferentiated 2iESCs (UD), followed by a decrease post-differentiation at D3 and D6 (Figure
153 1F). It is noteworthy that deacetylation of H3K27 at D6 post-differentiation is not succeeded by
154 H3K27 methylation at these sites. H3 occupancy shows no significant difference in enrichment in
155 various samples pre- and post-differentiation, further validating the significance of the observed
156 chromatin modification changes (Figure S1I).

157 Previous studies have shown that during enhancer silencing, histone demethylation of H3K4me1
158 and deacetylation of H3K27Ac by Lsd1-Mi2NURD- complex poises the chromatin for DNMT3A
159 activity (Petell et al., 2016). Therefore, we asked if DNA methylation at enhancer regions
160 maintained the repression of *Dnmt3b* post-differentiation. Methylation-dependent qPCR (MD-

161 qPCR) showed a significant gain of DNA methylation at distal and proximal enhancer regions on
162 D6 post-differentiation (Figure 1G). To directly test the role of DNMT3A and DNMT3L, we
163 compared DNA methylation in the WT, *Dnmt3a*$^{-/-}$, and *Dnmt3l*$^{-/-}$ cells. We observed that compared
164 to WT and *Dnmt3l*$^{-/-}$ cells, the *Dnmt3a*$^{-/-}$ cells showed a severe defect in gaining DNA methylation
165 (Figure 1G). The *Dnmt3b* promoter also harbors a CpG island (CGI) around TSS, and we asked
166 if DNA methylation spreads into the CGI. As previously reported for strong CGIs, the DNA
167 methylation levels decreased with increasing proximity to the *Dnmt3b* promoter CGI (Figure 1H).
168 However, unlike in the proximal and distal enhancers regions (Fig 1D), the CGI promoter region
169 showed a recovery of H3K27me3 at D6 post-differentiation, demonstrating that the PRC2 -
170 mediated mechanism maintains the repressed state of the *Dnmt3b* promoter (Figure 1I). Overall,
171 these data establish the activity of distal and proximal enhancers in regulating *Dnmt3b* expression
172 during 2i-ESC differentiation.

173 ***Dnmt3bas regulates the magnitude of Dnmt3b induction***

174 The divergent antisense (*as*) long non-coding RNA (lncRNA), *Dnmt3bas*, is a 2.8 kb transcript
175 that initiates 800 bps downstream of TSS in the *Dnmt3b* promoter (Figure S2A). Sequence
176 analysis of *Dnmt3bas* revealed a potential exon-intron structure, and structural modeling of the
177 spliced *Dnmt3bas* using RNA Fold webserver (ViennaRNA) showed a stem structure typical of
178 lncRNAs (Figure S2B). Based on the predicted exon-intron boundaries, we designed primers to
179 capture potential spliced and polyadenylated forms of *Dnmt3bas* (Figure S2A). An expected
180 unique band of nearly 716 bps, which corresponds to the size of spliced *Dnmt3bas*, confirmed
181 the splicing and polyadenylation of *Dnmt3bas* (Figure 2A). Subcellular localization assays showed
182 that *Dnmt3bas* is predominantly present in the nucleus (Figure 2B).

183 We first asked if there is a correlation between the expression of *Dnmt3b* and *Dnmt3bas* during
184 2i medium adaptation and differentiation of ESCs. We used exon-specific primers to detect the
185 expression of spliced *Dnmt3bas*, which also minimizes potential amplification from genomic

186 DNA contamination in the RNA samples (Figure S2C). The RT-qPCR specificity was ensured by
187 the absence of signal in the NRT (no reverse transcriptase) control and by visualizing the
188 amplified product as a single band on an agarose gel (Figure S2D). Expression analysis
189 showed that *Dnmt3b* was downregulated at passage P6 and maintained a basal level in 2i-
190 ESCs. Interestingly, *Dnmt3bas* expression constantly increased during the adaptation process
191 (Figure S2E). However, during 2i-ESC differentiation, the expression of *Dnmt3bas* was
192 downregulated concomitant with induction of the *Dnmt3b* (Figure 2C).

193 The coordinated yet contrasting expression pattern of the *Dnmt3b*/*Dnmt3bas* pair suggests a
194 potential role for *Dnmt3bas* in regulating *Dnmt3b* transcription. Therefore, we generated stable
195 ESCs lines expressing anti-*Dnmt3bas* shRNA (KD1 and KD2) or overexpressing (OE) spliced
196 and unspliced forms (spl and uns) of *Dnmt3bas* and successfully adapted them to 2i medium
197 shown by an increase in *Prdm14* expression in adapted cells (Figure S2F, G). Gene expression
198 analysis in the *Dnmt3bas* KD1 and KD2 cells showed a significant reduction of *Dnmt3bas* by
199 nearly 2.5-fold compared to the vector control (VC) cells. Conversely, *Dnmt3bas* OE cells
200 showed nearly 8-9-fold higher expression of *Dnmt3bas* compared to VC cells (Figure 2D).
201 Furthermore, cell fractionation analysis of the *Dnmt3bas* KD and OE cells showed a proportional
202 change in the *Dnmt3bas* transcript level in the cytoplasm and nucleus (Figure S2H), supporting
203 the localization of *Dnmt3bas* primarily in the nucleus. We also ruled out the potential
204 confounding impact of impaired pluripotency in the *Dnmt3bas* manipulated cell lines. Cell
205 morphology and gene expression analysis pre and post-differentiation show no significant
206 difference between the three cell lines (Figure S2I, J).

207 Next, we determined the effect of *Dnmt3bas* manipulations on *Dnmt3b* expression in the
208 *Dnmt3bas* KD and OE cell lines. The data showed no difference in *Dnmt3b* basal expression in
209 undifferentiated 2i-ESCs (Figure 2E). We next tested the effect on *Dnmt3b* induction post-
210 differentiation. Similar to our observation in Figure 1A, the VC cells showed a 15-fold induction

211 of *Dnmt3b* at D3 before reaching the basal level at D6 post-differentiation. Interestingly, in the
212 KD cells, the induction of *Dnmt3b* at D3 increased nearly 30-fold and returned to the basal level
213 at D6 post-differentiation. In OE cells, an opposite effect on *Dnmt3b* induction was observed,
214 with only a 7-fold increase in *Dnmt3b* expression on D3 post-differentiation. Moreover, the
215 repressive activity of *Dnmt3bas* was specific for only the spliced isoform since cells
216 overexpressing the unspliced *Dnmt3bas* behaved similarly to VC cells (Figure 2E). In addition,
217 this effect on *Dnmt3b* induction was rescued by overexpression of *Dnmt3bas* in KD cells (KD-
218 OE), confirming the trans activity of the *Dnmt3bas* transcript (Figure 2F). A similar effect on
219 Dnmt3b expression was observed in both KD1 and KD2 cells (Figure S2K); therefore, only KD1
220 cells were used for further investigation. We next asked if *Dnmt3bas* modulated the kinetics or
221 magnitude or both of *Dnmt3b* induction. A time-course experiment was performed to measure
222 the temporal increase in transcript levels of *Dnmt3b* every 24 hrs post differentiation. The data
223 were fit to a non-linear regression using GraphPad Prism. Whereas an apparent change in the
224 magnitude of induction was recorded, it peaked at the same time point in all three cell lines,
225 indicating the effect of *Dnmt3bas* on the magnitude of *Dnmt3b* induction (Figure 2G).

226 2iESC are hypomethylated, and genome-wide establishment of DNA methylation requires
227 activities of both DNMT3A and DNMT3B post-differentiation (Okano et al., 1999). We
228 investigated the potential impact of *Dnmt3bas* manipulations on the establishment of DNA
229 methylation. Analysis of global methylation using methylation-sensitive restriction showed a
230 delay in the gain of methylation in both KD and OE cells compared to VC cells (Figure S2L). We
231 used bisulfite sequencing to compare gain in DNA methylation of two Dnmt3b-specific target
232 regions on D2 post-differentiation (Yagi et al., 2020) (Figure 2H). A significant increase in DNA
233 methylation was observed in KD cells compared to the VC and OE cells, demonstrating the
234 effect of higher *Dnmt3b* expression on DNMT3B target methylation.

235 Collectively, these data confirm the role of the spliced *Dnmt3bas* transcript in *Dnmt3b*
236 transcriptional induction and suggest a mechanistic model in which the repressive effect of
237 *Dnmt3bas* maintains *Dnmt3b* promoter/proximal enhancer in the primed state in undifferentiated
238 cells to fine-tune the magnitude of *Dnmt3b* induction in response to differentiation signals.

239 ***Dnmt3bas modulates the chromatin modification state at Dnmt3b regulatory regions.***

240 To understand the mechanism of *Dnmt3bas* in regulating *Dnmt3b* induction, we measured
241 chromatin modifications, i.e., H3K4me1, H3K27me3, and H3K27Ac at *Dnmt3b* regulatory
242 regions during differentiation and compared changes in KD and OE cells to VC cells. In all three
243 cell lines, an increase in H3K4me1 was observed at both proximal and distal enhancer regions
244 at D3 post-differentiation compared to the undifferentiated (UD) cells (Figure 3A). Similarly, the
245 loss of H3K27me3 was accompanied by the gain of H3K27Ac at the proximal and distal
246 enhancer region in D3 cells (Figure 3B). Interestingly, we observed a lower enrichment of
247 H3K27Ac on D3 in OE cells than in KD and VC cells (Figure 3C), corresponding to the
248 alleviated induction of *Dnmt3b* gene expression (Figure 2F).

249 We next measured H3K27me3 and H3K27Ac close to CGI at the Dnmt3b promoter. Our data
250 showed that H3K27me3 demethylation is accompanied by H3K27 acetylation during the
251 differentiation of all three cell lines (Figure 3D, 3E). However, compared to the VC cells, we
252 observed a lower and a higher enrichment of H3K27me3 in undifferentiated KD and OE cells,
253 respectively (Figure 3D, S3A). Expectedly, an opposite trend in H3K27Ac was observed in
254 these cells (Figure 3E), conforming to the difference in Dnmt3b induction. The absence of
255 predicted changes in H3K27me3 at the distal enhancer in *Dnmt3bas* KD and OE cells is
256 possibly due to the low enrichment of this modification, limiting its detection. We also tested the
257 potential effect of *Dnmt3bas* on DNA methylation at the promoter and proximal enhancer (PE)
258 region. Similar to the VC cells, a gain of DNA methylation was observed in promoter regions

259 farther from the CGI that was not affected by changes in *Dnmt3bas* levels in KD and OE cells
260 (Figure 3F).

261 Based on the above data, we speculated that *Dnmt3bas* recruits the PRC2 complex to *Dnmt3b*
262 cis-regulatory regions, similar to several other lncRNAs known to escort the PRC2 complex to
263 their target sites (listed in (Schertzer et al., 2019; Statello et al., 2021)). The presence of PRC2
264 complex was confirmed by Suz12 ChIP, which shows strong enrichment at the Dnmt3b promoter.
265 In alignment with H3K27me3, significantly lower and higher Suz12 enrichment was observed in
266 the KD and OE cells, respectively, compared to VC cells (Figure 3G). This observation suggests
267 the role of *Dnmt3bas* in recruiting the PRC2 complex. To determine the interaction of the PRC2
268 complex with *Dnmt3bas*, we performed an RNA pull-down assay using *in vitro* transcribed
269 biotinylated *Dnmt3bas* and immunoblotted the precipitate for the PRC2 complex proteins. An
270 absence of a positive signal suggested either weak direct binding or indirect interaction of the
271 PRC2 complex mediated by other proteins such as hnRNPK (Pintacuda et al., 2017).
272 Immunoblotting confirmed a strong and specific interaction of hnRNPK with *Dnmt3bas* (Figure
273 S3B). Overall, these data demonstrate that manipulating *Dnmt3bas* levels significantly affects
274 PRC2 targeting and the deposition of H3K27me3 at the promoter/PE region, that in turn affects
275 the gain of H3K27Ac and *Dnmt3b* induction post-differentiation.

276 ***Dnmt3bas is localized at the Dnmt3b promoter and enhancer and affects E-P looping*.**

277 We performed a 3C assay in VC, KD, and OE cell lines to test the effect of *Dnmt3bas* on distal
278 enhancer-promoter interaction. The data show little or no effect on the interaction frequency of
279 *Dnmt3b* distal enhancer and promoter in the undifferentiated 2i-ESCs (Figure 4A). However, we
280 observed a higher interaction frequency between enhancer and promoter in KD cells than in VC
281 cells (Figure 4B). These data suggest that an increase in H3K27Ac at *Dnmt3b* regulatory
282 regions reinforces the E-P loop formation in KD cells, potentially affecting the induction level of
283 the *Dnmt3b* gene.

284 Given that *Dnmt3bas* affects H3K27Ac at the distal enhancer, we asked if *Dnmt3bas* RNA is
285 associated with the chromatin near the distal enhancer. We performed the Chromatin Isolation
286 by RNA purification (ChIRP) assay in WT and transgenic (VC, OE, and KD) 2iESCs pre- and
287 post-differentiation. Using probes specific to exon or intron regions of *Dnmt3bas*, RNA recovery
288 analysis showed high and specific recovery of the spliced *Dnmt3bas* from the RNA fraction of
289 undifferentiated and D3 differentiated cells (Figure 4C, S4A). From the DNA fraction,
290 approximately 10-fold higher enrichment of the *Dnmt3b* promoter region was measured
291 compared to the distal enhancer (Figure 4D). A significantly lower and higher enrichment of the
292 Dnmt3b promoter region was observed in KD and OE cells, respectively, compared to VC, and
293 no significant change was observed in the enrichment of the Dnmt3b distal enhancer region
294 (Figure 4E). These data confirm that spliced *Dnmt3bas* is located primarily at the *Dnmt3b*
295 promoter.

296 ***hnRNPL binds Dnmt3bas* at a CA repeat region in exon 2**

297 To determine the mechanism of *Dnmt3bas* in *Dnmt3b* promoter priming and transcriptional
298 induction, we performed an RNA pull-down assay to identify *Dnmt3bas* interacting proteins
299 using i*n vitro* transcribed biotinylated *Dnmt3bas* and control antisense-*Dnmt3bas* RNAs (Figure
300 5A). The bound proteins were visualized on a Coomassie-stained SDS-PAGE. A distinct protein
301 band at around 60 KDa was explicitly observed in the *Dnmt3bas* elution and was absent in the
302 control sample (Figure S5A). We performed mass spectrometry (MS) analysis of proteins from
303 control and experimental lanes within the excised fragment to identify proteins in the specific
304 band. The data from MS showed a strong enrichment of hnRNPL in the experimental sample.
305 The protein band was confirmed to be hnRNPL by immunoblotting the RNA pull-down samples
306 (Figure 5B). To examine the *in vivo* binding of hnRNPL to *Dnmt3bas*, we performed a western
307 blot analysis of the protein fraction from the *Dnmt3bas* ChIRP assay. The data showed a strong
308 signal of hnRNPL in the experimental sample that was absent in the RNase-treated control

309 sample (Figure 5C). ChIP assay using an anti-hnRNPL antibody showed significant and specific
310 enrichment of hnRNPL at the *Dnmt3b* promoter, confirming its *in vivo* binding at these sites
311 (Figure 5D).

312 hnRNPL binds CA repeats with high affinity (Smith et al., 2013), and *Dnmt3bas* contains two
313 clusters of CA-repeats within exon 2 spaced apart by about 50bps. To locate the hnRNPL
314 binding sites, we performed RNA pull-down assays using *Dnmt3bas* fragments (Figure 5E).
315 Compared to a weak binding in the exon 1 fragment (F1), strong hnRNPL binding was observed
316 in the intermediate and the exon 2 RNA fragments (F2, F3) containing both CA clusters (Figure
317 5F). Next, we systematically mutated the CA clusters in the full-length *Dnmt3bas* and used the
318 variants for the RNA pull-down assay. Variants 1 and 3 have different mutations in clusters 1
319 and 2, and variant 2 has mutations in only cluster 2. Whereas the hnRNPL binding of variant 2
320 is similar to that of WT *Dnmt3bas*, a very weak binding was detected for variants 1 and 3
321 (Figure 5G), indicating that hnRNPL predominantly binds to the cluster 1 site. Thus, we
322 conclude that hnRNPL specifically binds *Dnmt3bas* and is recruited to the *Dnmt3b* promoter
323 region.

324 ***Dnmt3bas* modulates alternative splicing of *Dnmt3b* through hnRNPL activity.**

325 Previous studies have shown that the RNA-binding protein hnRNPL regulates alternative
326 splicing (AS) (Cole et al., 2015; Hung et al., 2008; Preussner et al., 2012). Given that *Dnmt3bas*
327 recruits hnRNPL to the *Dnmt3b* promoter, we speculated that post-induction, the *Dnmt3bas*-
328 hnRNPL complex facilitates the interaction of hnRNPL with elongating RNA Pol II, which ferries
329 hnRNPL to alternatively spliced sites at the 3' end of the *Dnmt3b* transcript. First, we tested the
330 role of *Dnmt3bas* in the alternative splicing of *Dnmt3b. The* ratio of *Dnmt3b1:Dnmt3b6* was
331 determined using RT-PCR analysis in VC, KD, and OE cells cultured in the 2i medium (Figure
332 6A). *Dnmt3b1:Dnmt3b6* ratio in VC cells pre- and post-differentiation was as shown for WT
333 2iESCs in Figure 1B. *Dnmt3b6* is the predominant isoform in undifferentiated (UD) 2iESCs. Post

334 differentiation (D3) transcriptional induction of Dnmt3b was accompanied by increased exon
335 inclusion, thus transcribing *Dnmt3b1* as a major isoform. Although this trend was prevalent in
336 KD and OE cells, we observed a peculiar increase in the *Dnmt3b1*: *Dnmt3b6* ratio in OE cells
337 post-differentiation (Figure 6A). To test if increased exon inclusion was due to higher hnRNPL
338 recruitment in OE cells, we overexpressed *Dnmt3bas* variants with mutations in hnRNPL
339 binding sites in 2iESCs. Transgenic cell lines were differentiated, and alternative splicing of
340 *Dnmt3b* was analyzed at D3 post-differentiation. Compared to cells overexpressing WT
341 *Dnmt3bas*, the ratio of *Dnmt3b1*:*Dnmt3b6* in cells overexpressing variants was similar to that in
342 the VC cells (Figure 6B). Furthermore, suppression of hnRNPL expression in OE s-ESCs
343 (serum cultured) rescued the *Dnmt3b6:Dnmt3b1* ratio to that in VC s-ESCs (Figure S6A, 6C).
344 This data confirms the direct role of the hnRNPL/*Dnmt3bas* complex in regulating Dnmt3b
345 alternative splicing.

346 Together our data suggest that in *Dnmt3bas* OE cells, increased recruitment of hnRNPL at the
347 promoter increases the number of exon inclusion events. Previous studies have shown that the
348 interaction of SETD2 with hnRNPL and elongating RNA Pol II couples transcriptional elongation
349 and alternative splicing (Bhattacharya et al., 2021a; Bhattacharya et al., 2021b; Yuan et al.,
350 2009). We observed no significant change in the deposition of H3K36me3 at the 3' end of the
351 *Dnmt3b* gene in *Dnmt3bas* OE cells compared to the VC cells (Figure S6B), confirming that the
352 activities of SETD2 and hnRNPL are not dependent on their interaction with each other (Yuan et
353 al., 2009). However, this observation does not exclude the potential role of SETD2 in mediating
354 the interaction of hnRNPL with elongating Pol II.

355 ***A mechanistic model of Dnmt3bas***

356 Our study comprehensively examined the mechanism that regulates the spatiotemporal
357 expression of *Dnmt3b* during early development (Figure 7). The data revealed the unique role of
358 *Dnmt3bas* in transcriptional priming and coordinated activation of the *Dnmt3b* gene and

359 alternative splicing of the Dnmt*3b* transcript. In the undifferentiated 2i-ESCs, *Dnmt3bas*
360 maintains the *Dnmt3b* promoter in a primed state by regulating PRC2 activity. When
361 differentiation is triggered, *Dnmt3b* expression is induced by enhancement of E-P interaction
362 and deposition of H3K27Ac. Higher expression of *Dnmt3b* is also accompanied by increased
363 exon inclusion and switching of alternative splicing in favor of *Dnmt3b1* transcription. The
364 alternative splicing switch is facilitated by hnRNPL, a *Dnmt3bas* binding protein. At the
365 transcriptionally active *Dnmt3b* promoter, *Dnmt3bas* bridges the interaction of hnRNPL with
366 elongating RNA Pol II, ensuring its delivery to alternative splice sites. Following induction, the
367 post-differentiation repression of *Dnmt3b* is mediated by DNA methylation at proximal and distal
368 enhancers. Notably, the CGI promoter regains the H3K27me3 mark suggesting the role of a
369 lower but persistent expression of *Dnmt3bas*, which is essential for stabilizing the activity of the
370 PRC2 complex at the CGI promoter.

371 **Discussion**

372 Gene expression is controlled by the concerted activity of the transcriptional coactivator
373 complex and a permissive chromatin environment at its cis-regulatory elements. Additionally,
374 divergent long non-coding RNAs (lncRNA) regulate the expression of the nearby protein-coding
375 genes, including those crucial for normal development. They are often expressed from syntenic
376 regions among animal species (Dinger et al., 2008; Ponjavic et al., 2007), and widespread
377 antisense lncRNA transcription is evolutionarily conserved (Seila et al., 2008). LncRNAs act as
378 modulators of gene expression through multiple mechanisms, including the recruitment of
379 chromatin remodelers (Akhade et al.; Guttman et al.). Transcriptional regulation by lncRNAs can
380 be accomplished by either the transcript itself or by the act of transcription, which creates a
381 chromatin environment that influences the expression of the neighboring gene (Gil and Ulitsky,
382 2020). Many lncRNAs such as HOTAIR (Rinn et al., 2007), Kcnq1ot1 (Thakur et al., 2004), Air
383 (Sleutels et al., 2002), Evx1as(Luo et al., 2016), and Evf2as (Feng et al., 2006) are coordinately

384 transcribed with a protein-coding gene such that the pair is expressed from one transcriptional
385 locus (Engstrom et al., 2006). Several studies have used comparative expression analysis of
386 lncRNA/mRNA pairs to support a functional relationship between the divergent lncRNA and
387 associated protein-coding gene (Sigova et al., 2013). Our study characterized *Dnmt3bas* as a
388 promoter-associated divergent lncRNAs, expressed coordinately with *Dnmt3b* mRNA.
389 Mechanistically, *Dnmt3bas* acts in trans and regulates the induction and alternative splicing of
390 *Dnmt3b*.

391 ***Dnmt3b expression in ESC model system***

392 Serum-cultured ESCs are a mix of two interchangeable cell populations; naïve pluripotent cells
393 and epiblast stem cells. Epiblast stem cells are primed for differentiation, and their gene
394 expression profile shows the expression of early differentiation genes. In contrast, naïve ESCs
395 have high pluripotency genes expression (Tosolini and Jouneau, 2016; Ying et al., 2008).
396 Interestingly, in contrast to serum-ESCs, the expression of *Dnmt3b* is strongly downregulated in
397 2i-ESCs. Upon induction of differentiation, the transcript levels of *Dnmt3b* increase substantially
398 within a small window of 2-3 days, after which the *Dnmt3b* gene is completely repressed (Ficz et
399 al., 2013; Leitch et al., 2013). This is akin to the dynamic expression of *Dnmt3b* during early
400 embryogenesis that is restricted to the inner mass cells from E4.5-E8.5, after which *Dnmt3b*
401 expression is strongly downregulated in somatic lineages (Hirasawa and Sasaki, 2009; Okano
402 et al., 1999; Watanabe et al., 2002). We used 2i-adapted ESC differentiation to study the
403 dynamic regulation of *Dnmt3b* expression by the combined activity of its cis-regulatory elements
404 and *Dnmt3bas*. During 2i medium adaptation and ESC differentiation, we observed a
405 coordinated yet contrasting pattern of *Dnmt3b* and *Dnmt3bas* expression with the *Dnmt3b*
406 pattern mimicking the expression of *Dnmt3b* observed *in vivo*. The observation that *Dnmt3bas*
407 expression is lowest when the *Dnmt3b* gene is expressed at high levels suggests a potential
408 transcriptional interference mechanism wherein a high rate of sense transcription at the *Dnmt3b*

409 promoter will inhibit the antisense transcription of *Dnmt3bas* (Shuman, 2020). Nevertheless,
410 post-differentiation repression of *Dnmt3b* is not accompanied by an increase in *Dnmt3bas*
411 expression, suggesting a mechanism different from transcriptional interference and confirming
412 the regulatory role of *Dnmt3bas* in maintaining the primed state of the *Dnmt3b* promoter during
413 the pluripotent state.

414 ***Role of Dnmt3bas in Dnmt3b transcriptional induction***

415 Given that *Dnmt3bas* is expressed within the promoter of the *Dnmt3b* gene, genetic manipulations
416 using CRISPR/Cas9 could not be employed since it could have a confounding effect on *Dnmt3b*
417 expression. However, we observed a significant effect of *Dnmt3bas* on *Dnmt3b* expression by
418 using shRNA-mediated knockdown and overexpression of *Dnmt3bas* RNA in the 2i-ESCs.
419 Whereas the overexpression of *Dnmt3bas* suppresses the magnitude of *Dnmt3b* induction,
420 knockdown of *Dnmt3bas* has an opposite effect, complementing the observed inverse correlation
421 between their expression pre-induction and during *Dnmt3b* induction. The chromatin modification
422 state of the *Dnmt3b* cis-regulatory elements shows the impact of *Dnmt3bas* expression on
423 H3K27me3 at CGI promoter and enhancer elements. Our data suggest that *Dnmt3bas* recruits
424 the PRC2 complex to maintain the primed state of the *Dnmt3b* promoter and enhancer elements
425 in undifferentiated 2i-ESCs. In response to the differentiation signal, a concomitant loss of
426 H3K27me3 precedes the gain of H3K27Ac for activation of *Dnmt3b* enhancers, which engage
427 strongly with the promoter to facilitate transcriptional induction.

428 Some lncRNAs can help stabilize the E-P loop by interacting with components of the Mediator
429 complex like Med1 and Med12 (Luo et al., 2016) or cooperate with CTCF-mediated chromatin
430 interactions to affect the transcription of genes (Saldana-Meyer et al., 2019; Xiang et al., 2014;
431 Yang et al., 2015). However, we observed an increase in the enhancer-promoter (E-P) interaction
432 and H3K27Ac at the distal enhancer in *Dnmt3bas* KD cells, suggesting the role of *Dnmt3bas* in
433 stabilizing the repressive PRC2 complex binding. Furthermore, the proximity of the distal

434 enhancer to the Dnmt3b promoter in undifferentiated cells implies a dual role of the E-P loop, i) in
435 facilitating the recruitment of *Dnmt3bas* and PRC2 complex and ii) mediating a quick
436 transcriptional response to the differentiation signal.

437 Interestingly neither the expression of *Dnmt3bas* nor enrichment of H3K27me3 at distal regulatory
438 elements increased during the post-differentiation repression of *Dnmt3b*. Instead, we observed a
439 loss of H3K27Ac and a gain of DNA methylation in regions farther upstream, flanking the 5' end
440 of the CGI promoter. We also showed that DNA methylation was deposited by the
441 methyltransferase Dnmt3a and its allosteric activator protein, Dnmt3l. However, at the CGI
442 promoter, which is maintained in an unmethylated state post-differentiation, we observed an
443 increase in H3K27me3, suggesting the role of the PRC2 complex in maintaining the *Dnmt3b*
444 promoter in a repressed state post-differentiation. This observation also justifies the low but
445 significant expression of *Dnmt3bas* post-differentiation that could be involved in maintaining
446 H3K27me3 at the CGI. Interestingly, DNA methylation at the proximal enhancer region in the OE
447 cells also showed a distinguishable increase post-differentiation, suggesting positive
448 reinforcement of the repressive pathways. These observations are comparable with recent
449 studies showing that the lncRNA potency in spreading the PRC2 complex is tightly linked to
450 lncRNA abundance, genome architecture, and CpG island DNA (Schertzer et al., 2019). We
451 further showed that regulation of Dnmt3b expression by *Dnmt3bas* impacts the gain of DNA
452 methylation globally and at Dnmt3b target sites underscoring the importance of this mechanism.

453 ***Role of Dnmt3bas in Dnmt3b alternative splicing***

454 In ESCs, alternative splicing of the *Dnmt3b* transcript results in two main isoforms: *Dnmt3b6*,
455 exons 22 and 23 are excluded, and *Dnmt3b1*, the full-length transcript (Gowher et al., 2008).
456 Our data here show for the first time that *Dnmt3b* transcripts undergo a splicing switch in 2i-
457 ESCs post-differentiation. Previous studies reporting *Dnmt3b1* as a major isoform used ESCs
458 cultured in FBS. However, the 2i-ESCs, which are a homogenous population of cells in the

459 ground state of pluripotency, express catalytically inactive *Dnmt3b6* as the major isoform,
460 similar to the somatic expression of *Dnmt3b*3. These data suggest that besides downregulated
461 expression, alternative splicing of Dnmt3b contributes to the genome-wide loss of DNA
462 methylation in 2i-ESCs. Concurrently, basal transcription could also retain the Dnmt3b promoter
463 in a primed state for prompt activation. However, this would also necessitate the promoter
464 activation process to append a mechanism that facilitates exon inclusion to generate the full-
465 length *Dnmt3b1*.

466 Interestingly, among several unique proteins bound to *Dnmt3bas*, RNA pull-down assays
467 identified hnRNPL with the highest specific enrichment. The interaction of hnRNPL with
468 *Dnmt3bas* at the *Dnmt3b* promoter was also confirmed by ChIP and ChIRP assays. HnRNPL
469 functions as a regulator of alternative splicing (Cole et al., 2015; Hung et al., 2008; Preussner et
470 al., 2012), RNA stability (Hui et al., 2003), and transcriptional activation or repression in
471 partnership with multiple lncRNAs (Atianand et al., 2016; Li et al., 2014; Ruan et al., 2016).
472 Previous studies have shown that the binding of hnRNPs, including hnRNPK, hnRNPU, and U1
473 snRNP binding, facilitate chromatin tethering and nuclear retention of lncRNAs (Hacisuleyman
474 et al., 2016; Lubelsky and Ulitsky, 2018; Shukla et al., 2018; Yin et al., 2020). Med23 was also
475 shown to recruit hnRNPL to the promoter of genes, a role similar to *Dnmt3bas* (Huang et al.,
476 2012). These observations suggest that the nucleoprotein constitution of promoters can
477 determine both transcription and splicing outcomes (Cramer et al., 1997). Functional
478 characterization of *Dnmt3bas*/hnRNPL interaction showed increased inclusion of exons 22 and
479 23 in *Dnmt3b* transcript in the *Dnmt3bas* OE cells was reversed in cells overexpressing
480 *Dnmt3bas* with a mutation in the hnRNPL binding site. This observation suggests that hnRNPL
481 is the regulator of inducible exon inclusion, a process critical for expressing catalytically active,
482 *Dnmt3b1* during differentiation.

483 ***Implications of Dnmt3bas-hnRNPL interaction***

484 Recent studies have shown the interaction of SETD2 with hnRNPL and proposed that SETD2
485 hitchhikes to the elongating Pol II and transports hnRNPL to the splice sites as they emerge
486 during chain elongation(Yuan et al., 2009) (Bhattacharya et al., 2021a; Bhattacharya et al.,
487 2021b). Our study suggests that the recruitment of hnRNPL by *Dnmt3bas* to the promoter of
488 *Dnmt3b* facilitates hnRNPL- SETD2 transfer. Given that the RNA binding domain of hnRNPL,
489 RRM2, also interacts with SETD2, the interaction of hnRNPL with SETD2 and *Dnmt3bas* could
490 be mutually exclusive. This prediction is supported by the absence of SETD2 in the RIP/Mass
491 spectrometry analysis of *Dnmt3bas* binding proteins. Therefore, interaction choice could be
492 dictated by the proximity and binding strength of the RRM2 with RNA versus SETD2.

493 In contrast to hnRNPL, the knockdown of hnRNPI (PTBP1) notably increases exon inclusion in
494 the *Dnmt3b* mRNA (Gowher et al., 2012), suggesting that the antagonistic activity of
495 hnRNPI/hnRNPL potentially determines the splice site choice in *Dnmt3b* pre-mRNA. Both
496 proteins bind to similar polypyrimidine tracts (CA repeats) on RNA through their RRM domains
497 and interact with each other (Hahm et al., 1998). Interestingly PTBP1 is recruited to chromatin
498 by H3K36me3 (Luco et al., 2010), a modification deposited by SETD2. We observed an
499 increase in H3K36me3 post-differentiation (Fig S6B), which could contribute to hnRNPI/hnRNPL
500 recruitment at splice sites. However, the mechanism by which their antagonistic activity at
501 alternative splice sites is regulated is unknown. It would be interesting to determine the
502 mechanism of potential cross-talk between antagonist splice factors and chromatin modifiers
503 that fine-tunes the relative levels of the alternatively spliced isoforms in response to varying
504 physiological conditions. Also, given that *Dnmt3bas* acts in trans, future studies will determine
505 the potential global effect of its activity in regulating expression and alternative splicing of other
506 genes.

507 **Acknowledgments**

508 We are thankful to Gowher lab members for their discussions. This work was supported by NSF
509 award 1716678. In addition, we thank Dr. Tiaping Chen for Dnmt3a$^{-/-}$ and Dnmt3l$^{-/-}$ ESCs.
510 Finally, the authors gratefully acknowledge the Walter Cancer Foundation, DNA Sequencing
511 Facility, and support from the Purdue University Center for Cancer Research, P30CA023168.

512 **Authors Contributions**

513 M.S.D., I.K.M., M.H., S.M., M.C.H., H.C.W., N.E.B., M.C., M.E., and H.T. performed the
514 experiments. M.C.H., H.G.. analyzed the mass spectrometry data. M.S.D, I.K.M., and H.G.
515 wrote the manuscript

516 **Declaration of Interests**

517 None declared.

518 **Figure Legends**

519 **Figure 1. Proximal and distal enhancers regulate Dnmt3b induction.**

520 UD: undifferentiated; D1- D6: Days post-induction of differentiation; ESCs: embryonic stem
521 cells; s-ESC: serum cultured ESCs; RA: Retinoic Acid; LIF: Leukocyte Inhibitory factor; 2i:
522 Signaling pathway Inhibitors, CHIR99021 and PD184352; PE: proximal enhancer; Pro:
523 promoter; DE: Distal enhancer, CGI: CpG island; WT: wild type; 3a: Dnmt3a; 3l: Dnmt3L

524 (A) RT-qPCR of Dnmt3b during 2iESC differentiation as illustrated. The threshold cycle (Ct)
525 values were normalized to Gapdh, and expression is shown relative to that in UD cells. The data
526 show a steady increase in Dnmt3b expression up to D3, which decreases at D4 post-
527 differentiation.

528 (B) Illustration of Dnmt3b alternative exons, 22 and 23, and position of the primers used to
529 amplify the alternatively spliced isoforms, *Dnmt3b1* and *Dnmt3b6*. RT-PCR analysis *Dnmt3b*

530 alternative splicing in serum cultured (S-ESCs) and 2i cultured (2i-ESCs) cells pre and post-
531 differentiation.

532 (C) Chromatin conformation assay (3C) shows an interaction of the distal enhancer with the
533 promoter of Dnmt3b. The location of the distal enhancer and promoter in the Dnmt3b locus, the
534 3C PCR primers, and the corresponding HaeIII sites (tick marks) are shown. qPCR analysis
535 was done using the primer at the DE as an anchor (Chr2 position: 153466046), and interactions
536 with downstream sites were measured in 2iESC at undifferentiated and D3 post differentiation
537 state. Plotted are the relative interactions in arbitrary units of the Dnmt3b DE with six HaeIII
538 sites. The X-axis represents the chromosome 2 location (153465120- 153477120) of these
539 HaeIII sites. A significant increase in the interaction frequency was observed between DE and
540 Pro of the Dnmt3b gene at D3 post-differentiation.

541 (D, E, F, I) Chromatin immunoprecipitation (ChIP)-qPCR shows fold enrichment over input.
542 Histone modifications at Dnmt3b regulatory elements (D) H3K4me1 (E) H3K27Ac and (F, I)
543 H3K27me3 in 2iESCs pre- and post-differentiation. Concomitant with Dnmt3b induction, a
544 systematic increase and decrease in the H3K4me1 and H3K27Ac signal was observed post-
545 differentiation. Whereas H3K37me3 demethylation is maintained post differentiation at the
546 Pro/PE and DE, it is regained at the CGI region of the Pro, close to the TSS of the Dnmt3b
547 gene. P-values were derived from Student's t-test: *$p < 0.05$; **$p < 0.01$; ***$p < 0.005$.

548 (G, H) MD-qPCR was used to measure DNA methylation. The DNA was restricted using the
549 methylation-dependent enzyme MspJI which cuts at methylated cytosines. The specified
550 regions in the regulatory elements were amplified using the cleaved DNA as the template by
551 qPCR. The Cq values for differentiated samples were normalized to that of the undifferentiated
552 sample. An increase in the Cq value indicates a gain in DNA methylation. (G) Genomic DNA
553 was collected from the WT, Dnmt3a$^{-/-}$ and Dnmt3l$^{-/-}$ ESC cell lines pre-and post-differentiation.
554 DNA methylation analysis shows a reduced gain in both Dnmt3a$^{-/-}$ and Dnmt3l$^{-/-}$ cells. (H) DNA

555 methylation analysis in 2iESCs pre and post-differentiation at Dnmt3b Pro and CGI regions. The
556 tested CpG sites are represented on X-axis as base pairs upstream of the Dnmt3b TSS. The
557 data show a steady gain of DNA methylation corresponding to the distance away from the CGI,
558 which is maintained in an unmethylated state. Results are presented as normalized mean
559 values ± SEM for n = 3. See also Figure S1.

560 **Figure 2. Spatiotemporal expression of Dnmt3b in *Dnmt3bas* manipulated ESCs**

561 UD: undifferentiated; D1- D6: Days post-induction of differentiation; ESCs: embryonic stem
562 cells; VC: Vector control; KD: shRNA mediated knockdown of *Dnmt3bas*; OE: overexpression of
563 *Dnmt3bas* lncRNA; spl: spliced *Dnmt3bas*, uns: unspliced *Dnmt3bas*

564 (A) Ethidium bromide-stained agarose gel. RT-PCR of *Dnmt3bas* using exonic (lane 1) and
565 Oligo dT (lane 2) primers show a single band corresponding to the spliced transcript.

566 (B, C, D, E, F, G) RT-qPCR analysis of *Dnmt3bas* expression. (B) RT-qPCR of *Dnmt3bas* from
567 nuclear and cytosolic fractions of RNA showed about 2-fold higher enrichment in the nucleus
568 compared to the cytosol. In contrast, Dnmt3b and Gapdh mRNA transcripts showed a
569 significantly higher enrichment in cytosol compared to the nucleus. (C) RT-qPCR shows
570 *Dnmt3bas* expression in 2iESCs pre- and post-differentiation, with the highest expression in the
571 UD state. (D) RT-qPCR of *Dnmt3bas* from transgenic 2i-ESC lines expressing *Dnmt3bas*
572 shRNA (KD1, KD2), spliced (spl) and unspliced (uns) transcripts of *Dnmt3bas* (OE), and spliced
573 *Dnmt3bas* in KD cells (KD-OE). The Ct values were normalized to Gapdh, and expression is
574 shown relative to that in vector control (VC) cells. (E, F) RT-qPCR analysis of Dnmt3b
575 expression in Dnmt3bas manipulated transgenic 2i-ESCs, pre-and post-differentiation. (E) At
576 D3, the KD and OE cells showed significantly higher and lower induction than VC cells,
577 respectively. (F) In KD-OE cells, Dnmt3b induction is rescued to the level in VC cells at D3 post
578 differentiation. (G) Dnmt3b expression in VC, OE, and KD cell lines was measured every 24
579 hours post-differentiation. The data were fit to a non-linear regression in PRISM to estimate the

580 time of the Dnmt3b induction peak. P values were derived from the ANOVA test or Student's t-
581 test: *p < 0.05; **p < 0.01; ***p < 0.005.

582 (H) DNA methylation analysis using Bis-Seq. Bisulfite-treated genomic DNA from D2
583 differentiated cells was used to PCR amplify two Dnmt3b-specific target regions, CXXC5: chr18;
584 35858578 : 35858863, Rbm12b2; chr4;12113443 : 12114006. The amplicons were sequenced
585 on a high throughput sequencing platform (Wide-Seq), and the data were analyzed using
586 Bismark software. The box plot represents the range of percent DNA methylation at various
587 CpG sites in each target region. The median methylation at both targets is higher in KD cells
588 compared to VC cells. P values were calculated using Wilcoxon -matched pairs rank test: *p <
589 0.05; **p < 0.01; ***p < 0.005. Results are presented as normalized mean values ± SEM. See
590 also Figure S2.

591 **Figure 3. Chromatin modification at Dnmt3b regulatory elements in *Dnmt3bas***
592 **manipulated ESCs**

593 UD: undifferentiated; D3, D6: Days post-induction of differentiation; PE: proximal enhancer; Pro:
594 promoter; DE: Distal enhancer; CGI: CpG island; VC: Vector control; KD: shRNA mediated
595 knockdown of *Dnmt3bas*; OE: overexpression of *Dnmt3bas* lncRNA

596 (A, B, C, D, E, G) ChIP-qPCR assays show fold enrichment over input normalized to control.
597 Histone modifications at Dnmt3b regulatory elements (A) H3K4me1 (B, D) H3K27me3 and (C,
598 E) H3K27Ac pre- and D3 post-differentiation in VC, KD, and OE cells. (A) On D3 post-
599 differentiation, an increase in the H3K4me1 signal was observed in KD and OE cells, similar to
600 the VC cells in the Pro/PE and DE regions. (B, D) All cell lines show H3K27me3 demethylation
601 on D3 post-differentiation. However, a higher enrichment of H3K27me3 is observed in
602 undifferentiated (UD) OE cells at the Dnmt3b promoter, including PE and CGI regions. (C, E)
603 H3K27Ac shows an increase at D3 post differentiation, albeit less in OE cells at all the cis-
604 regulatory elements. A significantly higher enrichment in KD cells compared to VC cells is also

605 notable at the CGI region on D3 post-differentiation. (G) Fold enrichment of the PRC2 complex
606 component, Suz12, at the *Dnmt3b* promoter CGI region shows an opposite effect of *Dnm3bas*
607 OE and KD on Suz12 binding.

608 (F) DNA methylation at the Dnmt3b promoter was measured by MD-qPCR. After digestion of
609 genomic DNA from VC, KD, and OE cells pre and post-differentiation using the FspE1 enzyme,
610 the specified regions in the regulatory elements were amplified using qPCR. The Cq values for
611 differentiated samples were normalized to that of the VC-UD sample. An increase in the Cq
612 value indicates a gain in DNA methylation. The tested CpG sites are represented on X-axis as
613 base pairs upstream of the Dnmt3b TSS. The data show a steady gain of DNA methylation
614 corresponding to the distance away from the CGI, which is maintained in an unmethylated state.

615 p values were derived from ANOVA test: *$p < 0.05$; **$p < 0.01$; ***$p < 0.005$. Results are
616 presented as normalized mean values ± SEM. See also Figure S3.

617 **Figure 4. *Dnmt3bas* associates with Dnmt3b enhancers and influences E-P looping**

618 UD: undifferentiated; D3: Days post-induction of differentiation; PE: proximal enhancer; Pro:
619 promoter; DE: Distal enhancer; VC: Vector control; KD: shRNA mediated knockdown of
620 *Dnmt3bas*; OE: overexpression of *Dnmt3bas* lncRNA

621 (A, B) Chromatin interaction assay, 3C, shows an interaction of the distal enhancer with the
622 promoter of Dnmt3b. 3C assays were performed using undifferentiated and D3 differentiated
623 VC, KD, and OE cells. Primer positions were, as described in Figure 1 legend, and primer at DE
624 was used as bait. The data in (A) show no change in E-P interaction in the undifferentiated cells,
625 whereas in (B), a stronger interaction was observed in KD cells at D3 post-differentiation.

626 (C, D, E) ChIRP (chromatin isolation by RNA purification) was performed using *Dnmt3bas*-
627 specific biotinylated probes. The RNA and DNA fractions from the eluate were separated and
628 used to probe for (C) *Dnmt3bas* transcript and (D) Dnmt3b Pro/PE and DE regions,

629 respectively. (C) We observed a prominent recovery of *Dnmt3bas* compared to Gapdh mRNA.
630 (D) From the DNA fraction, the Pro/PE region of Dnmt3b enriched 100-180-fold, and DE
631 showed 10-15-fold recovery compared to a non-specific region in the mouse genome. (E) Fold
632 DNA recovery of Pro/PE and DE regions in *Dnmt3bas* KD and OE cells compared to that in the
633 VC cells. OE cells show a significantly high fold DNA, specifically of the Pro/PE region.

634 Results are presented as normalized mean values ± SEM. P values were derived from
635 Student's t-test: *p < 0.05; ****p < 0.0001. See also Figure S4.

636 **Figure 5. hnRNPL binds to a CA repeat region in exon 2 of *Dnmt3bas***

637 3bas: *Dnmt3bas* transcript, A-3bas: Antisense of *Dnmt3bas* transcript, bt-UTP: biotinylated
638 UTP, IN: Input, NC: negative control, E1: Exon1, M: Regions from Exon 1 and Exon 2, E2:
639 Exon2, Cluster 1 and Cluster 2: Predicted hnRNPL binding sites on *Dnmt3bas*, V1, V2: Variant
640 of *Dnmt3bas* transcript with substitutions in cluster 2 (2), and cluster 1 and 2 (1, 3) of hnRNPL
641 binding.

642 (A, E) Schematic showing the experimental design for in vitro transcription of (A) *Dnmt3bas*,
643 antisense control transcript, and (E) various *Dnmt3bas* fragments used for RNA pull-down
644 assays. The *in vitro* transcription was performed using biotinylated UTP and nuclear extract
645 from 2i-ESCs.

646 D) ChIP-qPCR assays show fold enrichment over the input of hnRNPL. NC is the control region
647 in the mouse genome. Results are presented as normalized mean values ± SEM. See also
648 Figure S5

649 (B, C F, G) Western Blot analysis of hnRNPL; (B) RNA pull-down assay showing specific
650 binding of hnRNPL to *Dnmt3bas* and not to antisense control transcript; (C) Protein fraction from
651 ChIRP assay showing hnRNPL, which was absent in eluate from RNAse treated sample. (F)
652 RNA pull-down assays using fragments of *Dnmt3bas* transcript show strong and specific binding

653 of hnRNPL to a region in Exon 2. (G) Variants of *Dnmt3bas* were used for RNA pull-down
654 assays, showing disrupted interaction of hnRNPL to variants 1 and 3 and not to variant 2

655 **Figure 6. hnRNPL regulates alternative splicing of Dnmt3b**

656 UD: undifferentiated; D3: Days post-induction of differentiation; VC: Vector control; KD: shRNA
657 mediated knockdown of *Dnmt3bas*; OE: overexpression of *Dnmt3bas* lncRNA; V1: Variant 1;
658 V3: variant 3; *Dnmt3b1*: Dnmt3b long isoform (exons 22 and 23 included); *Dnmt3b6*: Dnmt3b
659 short isoform(exons 22 and 23 excluded) s-ESC: serum cultured ESCs

660 (A) RT-PCR analysis of *Dnmt3b1* and *Dnmt3b6* expression amplified in the same reaction by
661 using primers flanking the AS exons. The illustration shows alternatively spliced exons 22 and
662 23, and red arrows represent the primers' position to amplify around the alternatively spliced
663 exons of the Dnmt3b gene. The bar graph shows the ratio of quantified band intensity *Dnmt3b1*
664 and *Dnmt3b6*. At D3 post differentiation, a switch to exon inclusion increases *Dnmt3b1*
665 expression relative to *Dnmt3b6*. The ratio of *Dnmt3b1:Dnmt3b6* is further increased in OE cells.
666 B) Ratio of *Dnmt3b1*/*Dnmt3b6* isoforms at D3 from cells overexpressing wildtype *Dnmt3bas*, V1
667 and V3 mutant *Dnmt3bas*, and vector control. The bar graph shows the ratio of quantified band
668 intensity. (C) siRNA mediated knockdown of hnRNPL in serum cultured ESCs. Control s-ESCs
669 (VC) show an almost equal ratio of *Dnmt3b1*:*Dnmt3b6* isoform expression, whereas Dnmt3bas
670 overexpressing (OE) cells show an enhanced exon inclusion. siRNA-mediated knockdown of
671 hnRNPL in OE cells restored the *Dnmt3b1*:*Dnmt3b6* isoform ratio to 1. Results are presented as
672 normalized mean values ± SEM. See also Figure S6.

673 **Figure 7. Model of epigenetic changes at pluripotency gene enhancers during stem cell**
674 **differentiation.** In the undifferentiated state (UD), *Dnmt3bas* maintains the *Dntm3b* promoter in
675 a primed state, where the proximal enhancer and promoter regions are characterized by
676 H3K27Me/3 chromatin modifications, facilitating basal *Dnmt3b* expression. In response to
677 differentiation signals (D3), *Dnmt3b* expression is induced via E-P interactions and the

678 deposition of H3K27Ac marks. In concert with induced *Dnmt3b* expression, a switch in
679 alternative splicing increases exon inclusion, promoting *Dnmt3b1* transcription. *Dnmt3bas*
680 directly bind and recruit hnRNPL, an obvious splicing factor, to the transcriptionally active
681 *Dnmt3b* promoter. Once at the promoter, hnRNPL hitchhikes RNA Pol II, potentially through an
682 adaptor protein, ensuring its delivery to *Dnmt3b* splice sites. Post-differentiation (D6), DNA
683 methylation by DNMT3A at the promoter and enhancers reduces the expression of *Dnmt3b*
684 back to basal levels. In particular, the CGI promoter regains H3K27me3 suggesting the role of a
685 lower but persistent expression of *Dnmt3bas*, which is required for stabilizing the activity of the
686 PRC2 complex at the CGI promoter.

687 **STAR Methods**

688 **Cell culture, adaptation, differentiation, and transgenic cell lines:**

689 As previously described by Alabdi et al., mouse embryonic stem cells (mESCs, E14Tg2A) were
690 cultured and maintained in gelatin-coated tissue culture plates. Differentiation of mESCs was
691 induced by plating $10X10^6$ cells in low attachment 10 cm Petri dishes with a concurrent
692 withdrawal of LIF. After Day 3, embryoid bodies were treated with 1μM Retinoic acid (RA), the
693 medium was replenished every day, cells were harvested each day, and samples were
694 collected for protein, RNA, DNA, and chromatin until Day 9.

695 CRISPR KO dnmt3a and dnmt3l cell lines were procured from Dr. Taiping Chen, MD Anderson.
696 Transgenic *Dnmt3bas* knockdown (KD) and overexpression (OE) cell lines were generated by
697 transfecting serum-cultured ESCs with pLKO.1 shRNA (Dharmacon) and pcDNA3.1*Dnmt3bas*
698 (spliced and unspliced). pcDNA3.1GFP transfected cells were used as control. After antibiotic
699 selection, the derived stable cell lines were adapted to the 2i culture conditions described below.

700 **2i Adaptation**

701 Serum-mESCs were seeded in a T-25 flask and passaged once before adapting them into 2i
702 media. Briefly, the serum-mESCs were washed with PBS and detached with trypsin. FBS was
703 added to inactivate the trypsin, DMEM/F12 media was added, and cells were pelleted. The cells
704 were rewashed to remove any traces of FBS and then plated and grown on gelatin-coated
705 tissue culture plates in 2i media (3μM CHIR99021 and 1μM PD0325901). The cells were
706 adapted until passage 10, and at every passage, the cells were harvested and checked for gene
707 expression and DNA methylation. The differentiation was induced by removing LIF from the
708 media, and at D3, 1μM RA was added, as explained earlier. The samples were harvested at
709 different time points for the analysis.

710 **Gene expression and alternative splicing analysis by qPCR and RT-PCR**

711 Briefly, total RNA was isolated using the TRIzol reagent (Invitrogen, 15596026) according to the
712 manufacturer's protocol. First, RNA samples were digested with DNAse (Roche, 04716728001)
713 at 37°C for two hours and purified using a Quick-RNA™ MiniPrep Plus Kit (ZymoReseach,
714 R1057). Then, reverse-transcription quantitative PCR (RT-qPCR) was performed either using
715 Verso One-Step RT-qPCR kits (Thermo Scientific, AB-4104A) or cDNA synthesized using the
716 Tetro cDNA Synthesis Kit (Bioline, BIO-65043). For Verso, we used 5-50ng of RNA per
717 reaction, and to synthesize cDNA, we used 1.2-2.5μg of RNA. cDNA was synthesized either
718 through gene-specific primers (GSP), random hexamers, or oligo (dT) as per the manufacturer's
719 instructions. Gene expression was calculated as $\Delta C_{t,}$ which is C_t(Gene)- C_t(*Gapdh or Beta-*
720 *actin*). Change in gene expression is reported as fold change relative to control undifferentiated
721 cells, which was set to 1, or in a $\log_2$ scale where values of undifferentiated cells were set to 0.
722 Standard deviations represent at least 2 technical and 2 biological replicates. SEM represents
723 the variance in average data with n=6 or more. The SD, SEM determination, and P-Value were
724 calculated using GraphPad Prism using ANOVA or paired Student T-test. To analyze alternative

725 splicing, a 1 step RT-PCR kit (Invitrogen,) was used to reverse transcribed Trizol purified and
726 DNAse (Roche, 04716728001) treated RNA from ESCs. We designed primers at exon-exon
727 boundaries (View primer list) such that product sizes were 200 – 500 bps long. Supplementary
728 Table S1 details the list of primers used in this study.

729 **Chromosome Conformation Capture Assay (3C).**

730 3C assays followed the protocol from (Hagege et al., 2007; Naumova et al., 2012) with a few
731 modifications. Murine 2i cells were crosslinked with 1% formaldehyde for 10 minutes at room
732 temperature. Chromatin was suspended in NEB buffer 2.1 and digested with 1000 units HaeIII
733 at 37°C overnight. Crosslinked fragments were ligated with 45 units T4 DNA ligase at 16 °C for
734 2 hours. A random ligation control template was generated using a BAC clone RP23-474F18
735 covering the Dnmt3b locus and digested with HaeIII and ligated with T4 ligase. Gapdh locus
736 was used as an endogenous control. Compared to a known concentration of E14 genomic DNA
737 by qPCR with primer pair GaploadF and GaploadR to determine 3C samples concentration.
738 According to the result, adjust each 3C sample to the same template amount for the following
739 quantitative PCR. Interaction frequency between anchor fragment (F1) and distant fragment
740 detection was done in triplicate by quantitative PCR using 3C products and BAC products as a
741 template and 3C primers. Primers position and sequence are indicated in (Fig 1) and Table S1.
742 The relative interaction frequency of each fragment to anchor was calculated as $2^{(Ct\ BAC\ -Ct\ 3C)}$. P-
743 values were calculated using GraphPad Prism using paired Student T-test.

744 **RNA-Pulldown and hnRNPL binding assays**

745 The WT and mutant *Dnmt3bas* templates for *in vitro* transcription assays were obtained by PCR
746 using primers containing the T7 promoter sequence (View primer list). Biotin-labeled *Dnmt3bas*
747 transcripts, *Dnmt3bas* antisense, and *Dntm3bas* variants 1, 2, and 3 were transcribed *in vitro*
748 using the T7 RNA polymerase (ThermoFisher Scientific, AM1333) with the following

749 modifications. Unlabeled ATP, GTP, and CTP were used at a concentration of 7.5 mM, except
750 for unlabeled UTP, which was used at 5.63 mM. Notably, the reaction was supplemented with
751 1.8 mM biotin-UTP (Roche, 11093070910). The transcripts were immobilized on streptavidin
752 beads and incubated with pre-cleared nuclear extract from 2i-ESCs for 45 mins at 4 ^{0}C.
753 Following washes, magnetic beads were boiled for 5 mins in the SDS-loading buffer as
754 previously described (Panda et al., 2016). Eluates were analyzed using Coomassie staining and
755 Western blot.

756 **Subcellular fractionation**

757 20 million mESCs were harvested for the subcellular fractionation, according to (Pandya-Jones
758 and Black, 2009; Wuarin and Schibler, 1994) protocol. Briefly, the cells were trypsinized and
759 centrifuged at low speed at RT for 5min. Cells were lysed by adding the NP-40 lysis buffer for 5
760 mins. The samples were centrifuged and the supernatant was saved as the cytosolic fraction.
761 The pellet was rinsed with the lysed buffer, to remove any cytoplasmic leftover. The pellet was
762 then resuspended in glycerol buffer by gentle flicking. This was followed by the addition of nuclei
763 lysis buffer. After 2 minutes of incubation, the sample was centrifuged and the supernatant
764 taken as the soluble nuclear fraction/nucleoplasm. Part of the fractions was used to perform the
765 western blot, and the remaining fraction was used to isolate the RNA for RT-qPCR analysis.

766 **Chromatin Isolation by RNA Purification (ChIRP)**

767 Chromatin Isolation by RNA Purification (ChIRP) was performed by following (Au - Chu et al.,
768 2012). Briefly > 20 million cells were grown and crosslinked 1% glutaraldehyde at room
769 temperature, followed by quenching for 5 minutes. The cell pellets were flash-frozen in liquid
770 nitrogen and stored at -80 °C indefinitely. The cells were thawed at room temperature and
771 dislodged. For 100mg of cell pellet, we used 1ml of lysis buffer containing Protease Inhibitor
772 cocktail, PMSF, and SUPERase•In™ RNase Inhibitor (Invitrogen). The cells were sonicated
773 using a Bioruptor (Diagnode) in 15 ml tubes for 2-3 hours. The sonicated sample was

774 centrifuged, and the supernatant was hybridized with the biotinylated DNA probes specific to
775 lncRNA, *Dnmt3bas*, for 4 hours. In the meantime, C-1 magnetic beads were washed and added
776 to the probe-sample mix. The complex was incubated at 37°C for 30 minutes and then washed
777 5 times with the 1ml wash buffer. The beads were resuspended in the final wash, and 100ul of
778 the sample was kept for RNA purification. The complex was processed accordingly for the
779 downstream analysis. For RNA purification, the bead complex was resuspended in TriZol, and
780 for DNA isolation, the complex was reverse crosslinked and RNase treated. RNA samples were
781 used to determine fold recovery of *Dnmt3bas* lncRNA by RT-qPCR. The purified ChIRP-DNA
782 was used as a template to determine the enrichment of the genomic region of interest by qPCR.
783 The bead complex was treated with a biotin elution buffer to isolate proteins (Au - Chu et al.,
784 2012) and immunoblotted to identify proteins of interest. Table S2 lists sequences of probes
785 used in this study.

786 **DNA methylation analysis**

787 *DNA Methylation-Dependent qPCR Assay (MD-qPCR) :* Genomic DNA (gDNA) was purified
788 using the standard phenol-chloroform method. The extracted gDNA was treated with RNAse
789 (Roche) overnight at 37 C. Following another round of Phenol-Chloroform DNA extraction,
790 gDNA was subjected to FspE1 (NEB, R0662S) digestion overnight at 37 C. The digested gDNA
791 was purified by the Phenol-Chloroform method and quantified using the NanoDrop 3300
792 fluorospectrometer through PicoGreen dye according to the manufacturer's protocol (Life
793 Technologies, P11495). Quantitative PCR was performed using an equal amount of DNA for
794 each sample. The change in DNA methylation is represented by relative fold change in the Cq
795 value as follows: 2ˆ(Cq(U)-Cq(I)), where Cq(U) is the Cq for the undifferentiated ESC sample,
796 and Cq(I) represents day 3 or day 7 differentiated ESCs. The primers used for DNA
797 methylation-dependent qPCR analysis have been previously described [30]. Standard
798 deviations represent three technical and two biological replicates.

799 *DNA Methylation-Dependent Restriction digest (MDR):* Purified genomic DNA was subjected to
800 methylation-sensitive restriction by Hpa II and methylation-insensitive restriction by Msp I
801 overnight at 37 C. Samples were loaded on 0.8% Agarose gel in TAE buffer and bands
802 visualized by Ethidium bromide staining. A smear in the Hpa II digestion lane indicates global
803 loss of DNA methylation.

804 *Bisulfite Sequencing:* Bisulfite sequencing was performed by using the EpiTect Fast Bisulfite
805 Conversion Kit (Qiagen, 59802) according to the manufacturer's protocol. Bisulfite-converted
806 DNA was PCR-amplified using published methods (Tremblay et al., 1997) and sequenced using
807 Illumina Wide-SEQ run, which generated over 5K paired-end reads for each sample. The reads
808 were then mapped by Bowtie2 and analyzed by Bismark for DNA methylation. Instances of
809 methylated and unmethylated CpG were quantified and summed to an overall percent
810 methylation for each gene with standard deviations. The significance was calculated by
811 Wilcoxon -matched pairs rank test using GraphPad Prism. See Table S2 for primers used for
812 bisulfite sequencing.

813 **Chromatin Immunoprecipitation**

814 ChIP was performed as described (Petell et al., 2016). Briefly, nuclei were isolated from the x-
815 linked cells and were sonicated using Bioruptor (Diagnode), according to the manufacturer's
816 protocol. A total of 8µg of sheared crosslinked chromatin was incubated with 8µg of antibody
817 pre-loaded on a 1:1 ratio of protein A and protein G magnetic beads (Life Technologies, 10002D
818 and 10004D, respectively). After washing the beads, the samples were eluted in 1% SDS, 10
819 mM EDTA, 50 mM Tris-HCl, pH 8.0. Crosslinking was reversed by incubation at 65°C for 30 min
820 with shaking. Samples were treated with RNase (Roche, 11119915001) for 2 h at 37°C, and
821 subsequently treated with Proteinase K (Worthington, LS004222) for 2 h at 55°C. DNA was
822 purified by phenol: chloroform extraction followed by ethanol precipitation and quantified using
823 PicoGreen (Life Technologies, P11495) and NanoDrop 3300 fluorospectrometer. qPCR and

824 data analysis were performed as previously described (Petell et al., 2016). Enrichment was
825 calculated as follows = Ct (IN)-Ct (IP) and the fold enrichment over input = 2^ [Ct (IN)-Ct (IP)].
826 Fold change was calculated by normalizing the fold enrichment at a specific site to that at the
827 control region (Chr 17: 13821873- 13821988). The significance of the change was determined
828 via *p*-value, which was calculated by GraphPad Prism using Student's *t*-test. Supplementary
829 Table S4 lists sequences of primers used.

830 **Western blot**

831 Standard western blot analysis was conducted on nuclear protein extracts and RNA-pulldown
832 eluates using anti-hnRNP L, 1:1000 (Abcam, ab32680), anti-hnRNP K, 1:1000 (Abclonal,
833 A1701), and anti-rabbit, 1:40,000 (Jackson Immunoresearch, 111-035-003).
834 Chemiluminescence was performed according to the manufacturer's protocol (Thermo-Fisher
835 Scientific 34580). For Dnmt3b expression, Protein samples were purified using standard RIPA
836 protein purification (Peach et al., 2015), and blotted with anti-Dnmt3b antibodies (sc-20704),
837 and β-actin (sc-47778) as a loading control. Images were taken using the ChemiDoc MP
838 imaging system (Biorad, 170001402).

839 **Supplementary figures legends**

840 **Figure S1. Proximal and distal enhancers regulate Dnmt3b induction**

841 s-ESCs: serum cultured embryonic stem cells; 2i-ESCs: 2i cultured embryonic stem cells 2i:
842 Signaling pathway Inhibitors, CHIR99021, and PD184352; UD: undifferentiated; D3, D6: Days
843 post-induction of differentiation: U: Uncut; H: Hpa II cut; M: Msp I cut

844 (A, E, F) Relative expression analysis by RT-qPCR of A) various early developmental genes in
845 2iESCs compared to expression in s-ESCs. E) Relative expression of pluripotency and
846 differentiation genes during 2i-ESC differentiation. The expression of genes in undifferentiated
847 cells was set to 0.

848 F) Dnmt3b expression in s-ESC pre and post-differentiation. The Ct values were normalized to
849 Gapdh, and expression is shown relative to that in UD cells. The data are an average and
850 standard deviation of three biological replicates.

851 (B) Alkaline phosphatase staining and SSEA-1 immunofluorescence of s-ESCs and 2i-ESCs. A
852 positive signal indicates pluripotency, which is strong in 2i-ESCs. The scale bar is 100 μm.

853 (C) DNA methylation analysis. Genomic DNA from 2iESC and s-ESCs was digested with
854 restriction enzymes Hpa II, which cuts unmethylated DNA at the 5'-CCGG-3' site, and MspI,
855 which cuts DNA at the same site irrespective of the DNA methylation.

856 (D) Bright field microscopy showing changes in cell morphology as 2i-ESCs differentiate.

857 G) Western blot showing the expression of Dnmt3b alternative splicing isoforms in
858 undifferentiated (UD) ESCs, Day 3 and Day 6 post-differentiation (D3 and D6, respectively)
859 cells. β-actin was used as the loading control.

860 H) Schematic of the Dnmt3b gene showing the position of the promoter-associated lncRNA
861 *Dnmt3bas* and upstream enhancer.

862 F) ChIP-qPCR assays show fold enrichment over the input of H3.

863 **Figure S2. Spatiotemporal expression of Dnmt3b in *Dnmt3bas* manipulated ESCs**

864 (A) Illustration of Dnmt3b promoter flanking regions shows the relative position, exon/intron
865 structure, and size of unspliced and spliced transcripts of the lncRNA *Dnmt3bas*, which is
866 transcribed in an antisense direction within the Dnmt3b promoter.

867 (B) Predicted minimum free energy structure of spliced *Dnmt3bas* transcript, determined using
868 ViennaRNA RNA Fold webserver. The structure is colored by base-pairing probabilities. For
869 unpaired regions, the color denotes the probability of being unpaired, from blue to red going
870 from the highest to the lowest.

871 C) Relative expression of various genes in 2i-ESCs compared to s-ESCs. The expression of
872 each gene in s-ESCs was set to 1.

873 D) Ethidium bromide-stained 6% acrylamide gel showing a specific amplification in the qRT-
874 PCR reactions with no signal in the reactions without Reverse Transcriptase (NRT).

875 E) Relative gene expression of Dnmt3b and *Dnmt3bas* during adaptation (P5-P10) of s-ESCs to
876 2i medium conditions.

877 F) Illustration of the transgenic cell line generation and adaptation to 2i media conditions.

878 G) The bar graph shows an increase in the expression of *Prdm14,* indicating successful
879 adaptation to 2i media conditions.

880 H) RT-qPCR of *Dnmt3bas* from nuclear and cytosolic RNA fractions from VC, KD and OE cell
881 lines showed about 2 fold higher enrichment in the nucleus compared to the cytosol and a
882 proportional increase in both nuclear and cytoplasmic fractions. Dnmt3b and Gapdh were used
883 as mRNA control, showing higher enrichment in the cytosol than in the nucleus.

884 I) Brightfield microscopy images of transgenic VC, KD, and OE cells pre and post-differentiation.

885 J) Relative expression of master pluripotency genes and differentiation-specific genes pre and
886 post-differentiation of the transgenic cell lines, VC, KD, OE.

887 K) Dnmt3b induction in a transgenic cell line expressing Dnmt3bas shRNA (KD2) during
888 differentiation.

889 L) DNA methylation analysis. Genomic DNA from transgenic VC, KD and OE cells was digested
890 with restriction enzymes Hpa II, which cuts unmethylated DNA at the 5'-CCGG-3' site, and MspI,
891 which cuts DNA at the same site irrespective of the DNA methylation. In undifferentiated cells
892 hypomethylated genome is fully digested by Hpa II. However, the post-differentiation gain of
893 DNA methylation protects against digestion by Hpa II prominently in VC cells and less in KD and
894 OE cells.

895 **Figure S3. Chromatin modification at Dnmt3b regulatory elements in *Dnmt3bas***
896 **manipulated ESCs**

897 A) ChIP-qPCR assay showing fold enrichment of H3K27me3 histone modification at Dnmt3b
898 regulatory elements.

899 B) Schematic showing the experimental design for in vitro transcription of *Dnmt3bas* and
900 antisense control transcript. The in vitro transcription was performed using biotinylated UTP and
901 nuclear extract from 2i-ESCs. The eluted proteins were analyzed on Western blot to identify
902 hnRNPK and Suz 12.

903 **Figure S4. *Dnmt3bas* associates with Dnmt3b enhancers and influences E-P looping**

904 ChIRP was performed using *Dnmt3bas* biotinylated probes specific for spliced and unspliced
905 transcripts. The RNA fraction from the eluate was separated and used to probe for spliced and
906 unspliced *Dnmt3bas* transcript. The data show a 10-fold higher enrichment of spliced transcripts
907 than the unspliced ones.

908 **Figure S5. hnRNPL binds to a CA repeat region in exon 2 of *Dnmt3bas***

909 Coomassie-stained gel showing proteins eluted after RNA pull-down using *Dnmt3bas* or anti-
910 *Dnmt3bas* control transcript. The boxes represent the gel slices that were used for the
911 extraction of proteins and detection by mass spectrometry. A prominent band is visible in the
912 *Dnmt3bas* lane compared to the control transcript.

913 **Figure S6. *Dnmt3bas* associates with Dnmt3b enhancers and influences E-P looping**

914 (A) Western blot showing the expression of hnRNPL in serum cultured ESC overexpressing
915 *Dnmt3bas* (OE), treated with control siRNA or siRNA to knock down hnRNPL expression.
916 GAPDH was used as the loading control.

917 (B) ChIP-qPCR assay showing fold enrichment of H3K36me3 histone modifications at the
918 Dnmt3b gene locus.

919 **Table S1. Primers used in this study.**

920 A list of all PCR primers used in this study (5' to 3'), separated by technique

921 **Table S2. ChIRP probes used in this study.**

922 A list of all ChIRP probes used in this study (5' to 3') with 3' biotin modification

923 **References**

924 Akhade, V.S., Pal, D., and Kanduri, C. (2017). Long Noncoding RNA: Genome Organization and
925 Mechanism of Action. Adv Exp Med Biol *1008*, 47-74.

926 Atianand, M.K., Hu, W., Satpathy, A.T., Shen, Y., Ricci, E.P., Alvarez-Dominguez, J.R., Bhatta, A.,
927 Schattgen, S.A., McGowan, J.D., Blin, J.*, et al.* (2016). A Long Noncoding RNA lincRNA-EPS Acts as a
928 Transcriptional Brake to Restrain Inflammation. Cell *165*, 1672-1685.

929 Au - Chu, C., Au - Quinn, J., and Au - Chang, H.Y. (2012). Chromatin Isolation by RNA Purification (ChIRP).
930 JoVE, e3912.

931 Bhattacharya, S., Levy, M.J., Zhang, N., Li, H., Florens, L., Washburn, M.P., and Workman, J.L. (2021a).
932 The methyltransferase SETD2 couples transcription and splicing by engaging mRNA processing factors
933 through its SHI domain. Nat Commun *12*, 1443.

934 Bhattacharya, S., Wang, S., Reddy, D., Shen, S., Zhang, Y., Zhang, N., Li, H., Washburn, M.P., Florens, L.,
935 Shi, Y.*, et al.* (2021b). Structural basis of the interaction between SETD2 methyltransferase and hnRNP L
936 paralogs for governing co-transcriptional splicing. Nat Commun *12*, 6452.

937 Cole, B.S., Tapescu, I., Allon, S.J., Mallory, M.J., Qiu, J., Lake, R.J., Fan, H.Y., Fu, X.D., and Lynch, K.W.
938 (2015). Global analysis of physical and functional RNA targets of hnRNP L reveals distinct sequence and
939 epigenetic features of repressed and enhanced exons. RNA *21*, 2053-2066.

940 Cramer, P., Pesce, C.G., Baralle, F.E., and Kornblihtt, A.R. (1997). Functional association between
941 promoter structure and transcript alternative splicing. Proc Natl Acad Sci U S A *94*, 11456-11460.

942 Derrien, T., Johnson, R., Bussotti, G., Tanzer, A., Djebali, S., Tilgner, H., Guernec, G., Martin, D., Merkel,
943 A., Knowles, D.G.*, et al.* (2012). The GENCODE v7 catalog of human long noncoding RNAs: analysis of
944 their gene structure, evolution, and expression. Genome Res *22*, 1775-1789.

945 Dinger, M.E., Pang, K.C., Mercer, T.R., and Mattick, J.S. (2008). Differentiating protein-coding and
946 noncoding RNA: challenges and ambiguities. PLoS computational biology *4*, e1000176.

947 Duymich, C.E., Charlet, J., Yang, X., Jones, P.A., and Liang, G. (2016). DNMT3B isoforms without catalytic
948 activity stimulate gene body methylation as accessory proteins in somatic cells. Nat Commun *7*, 11453.

949 Engstrom, P.G., Suzuki, H., Ninomiya, N., Akalin, A., Sessa, L., Lavorgna, G., Brozzi, A., Luzi, L., Tan, S.L.,
950 Yang, L.*, et al.* (2006). Complex Loci in human and mouse genomes. PLoS genetics *2*, e47.

951 Esteller, M. (2005). Aberrant DNA methylation as a cancer-inducing mechanism. Annual review of
952 pharmacology and toxicology *45*, 629-656.

953 Feng, J., Bi, C., Clark, B.S., Mady, R., Shah, P., and Kohtz, J.D. (2006). The Evf-2 noncoding RNA is
954 transcribed from the Dlx-5/6 ultraconserved region and functions as a Dlx-2 transcriptional coactivator.
955 Genes Dev *20*, 1470-1484.

956 Ficz, G., Hore, T.A., Santos, F., Lee, H.J., Dean, W., Arand, J., Krueger, F., Oxley, D., Paul, Y.L., Walter, J.*, et*
957 *al.* (2013). FGF signaling inhibition in ESCs drives rapid genome-wide demethylation to the epigenetic
958 ground state of pluripotency. Cell Stem Cell *13*, 351-359.

959 Gil, N., and Ulitsky, I. (2020). Regulation of gene expression by cis-acting long non-coding RNAs. Nat Rev
960 Genet *21*, 102-117.

961 Gopalakrishnan, S., Sullivan, B.A., Trazzi, S., Della Valle, G., and Robertson, K.D. (2009). DNMT3B
962 interacts with constitutive centromere protein CENP-C to modulate DNA methylation and the histone
963 code at centromeric regions. Human molecular genetics *18*, 3178-3193.

964 Gowher, H., Brick, K., Camerini-Otero, R.D., and Felsenfeld, G. (2012). Vezf1 protein binding sites
965 genome-wide are associated with pausing of elongating RNA polymerase II. Proc Natl Acad Sci U S A *109*,
966 2370-2375.

967 Gowher, H., and Jeltsch, A. (2002). Molecular enzymology of the catalytic domains of the Dnmt3a and
968 Dnmt3b DNA methyltransferases. The Journal of biological chemistry *277*, 20409-20414.

969 Gowher, H., Stuhlmann, H., and Felsenfeld, G. (2008). Vezf1 regulates genomic DNA methylation
970 through its effects on expression of DNA methyltransferase Dnmt3b. Genes Dev *22*, 2075-2084.

971 Greenberg, M.V.C., and Bourc'his, D. (2019). The diverse roles of DNA methylation in mammalian
972 development and disease. Nature Reviews Molecular Cell Biology *20*, 590-607.

973 Guil, S., and Esteller, M. (2009). DNA methylomes, histone codes and miRNAs: tying it all together. The
974 international journal of biochemistry & cell biology *41*, 87-95.

975 Guo, C.J., Ma, X.K., Xing, Y.H., Zheng, C.C., Xu, Y.F., Shan, L., Zhang, J., Wang, S., Wang, Y., Carmichael,
976 G.G.*, et al.* (2020). Distinct Processing of lncRNAs Contributes to Non-conserved Functions in Stem Cells.
977 Cell *181*, 621-636 e622.

978 Guttman, M., Amit, I., Garber, M., French, C., Lin, M.F., Feldser, D., Huarte, M., Zuk, O., Carey, B.W.,
979 Cassady, J.P.*, et al.* (2009). Chromatin signature reveals over a thousand highly conserved large non-
980 coding RNAs in mammals. Nature *458*, 223-227.

981 Guttman, M., Donaghey, J., Carey, B.W., Garber, M., Grenier, J.K., Munson, G., Young, G., Lucas, A.B.,
982 Ach, R., Bruhn, L.*, et al.* (2011). lincRNAs act in the circuitry controlling pluripotency and differentiation.
983 Nature *477*, 295-300.

984 Hacisuleyman, E., Shukla, C.J., Weiner, C.L., and Rinn, J.L. (2016). Function and evolution of local repeats
985 in the Firre locus. Nat Commun *7*, 11021.

986 Hagege, H., Klous, P., Braem, C., Splinter, E., Dekker, J., Cathala, G., de Laat, W., and Forne, T. (2007).
987 Quantitative analysis of chromosome conformation capture assays (3C-qPCR). Nat Protoc *2*, 1722-1733.

988 Hahm, B., Cho, O.H., Kim, J.E., Kim, Y.K., Kim, J.H., Oh, Y.L., and Jang, S.K. (1998). Polypyrimidine tract-
989 binding protein interacts with HnRNP L. FEBS Lett *425*, 401-406.

990 Hirasawa, R., and Sasaki, H. (2009). Dynamic transition of Dnmt3b expression in mouse pre- and early
991 post-implantation embryos. Gene Expr Patterns *9*, 27-30.

992 Huang, Y., Li, W., Yao, X., Lin, Q.J., Yin, J.W., Liang, Y., Heiner, M., Tian, B., Hui, J., and Wang, G. (2012).
993 Mediator complex regulates alternative mRNA processing via the MED23 subunit. Mol Cell *45*, 459-469.

994 Hui, J., Reither, G., and Bindereif, A. (2003). Novel functional role of CA repeats and hnRNP L in RNA
995 stability. RNA *9*, 931-936.

996 Hung, L.H., Heiner, M., Hui, J., Schreiner, S., Benes, V., and Bindereif, A. (2008). Diverse roles of hnRNP L
997 in mammalian mRNA processing: a combined microarray and RNAi analysis. RNA *14*, 284-296.

998 Huntriss, J., Hinkins, M., Oliver, B., Harris, S.E., Beazley, J.C., Rutherford, A.J., Gosden, R.G., Lanzendorf,
999 S.E., and Picton, H.M. (2004). Expression of mRNAs for DNA methyltransferases and methyl-CpG-binding
1000 proteins in the human female germ line, preimplantation embryos, and embryonic stem cells. Molecular
1001 reproduction and development *67*, 323-336.

1002 Ishida, C., Ura, K., Hirao, A., Sasaki, H., Toyoda, A., Sakaki, Y., Niwa, H., Li, E., and Kaneda, Y. (2003).
1003 Genomic organization and promoter analysis of the Dnmt3b gene. Gene *310*, 151-159.

1004 Jinawath, A., Miyake, S., Yanagisawa, Y., Akiyama, Y., and Yuasa, Y. (2005). Transcriptional regulation of
1005 the human DNA methyltransferase 3A and 3B genes by Sp3 and Sp1 zinc finger proteins. The
1006 Biochemical journal *385*, 557-564.

1007 Kulis, M., and Esteller, M. (2010). DNA methylation and cancer. Advances in genetics *70*, 27-56.

1008 Leitch, H.G., McEwen, K.R., Turp, A., Encheva, V., Carroll, T., Grabole, N., Mansfield, W., Nashun, B.,
1009 Knezovich, J.G., Smith, A.*, et al.* (2013). Naive pluripotency is associated with global DNA
1010 hypomethylation. Nature structural & molecular biology *20*, 311-316.

1011 Li, Z., Chao, T.C., Chang, K.Y., Lin, N., Patil, V.S., Shimizu, C., Head, S.R., Burns, J.C., and Rana, T.M. (2014).
1012 The long noncoding RNA THRIL regulates TNFalpha expression through its interaction with hnRNPL. Proc
1013 Natl Acad Sci U S A *111*, 1002-1007.

1014 Lubelsky, Y., and Ulitsky, I. (2018). Sequences enriched in Alu repeats drive nuclear localization of long
1015 RNAs in human cells. Nature *555*, 107-111.

1016 Luco, R.F., Pan, Q., Tominaga, K., Blencowe, B.J., Pereira-Smith, O.M., and Misteli, T. (2010). Regulation
1017 of alternative splicing by histone modifications. Science *327*, 996-1000.

1018 Luo, S., Lu, J.Y., Liu, L., Yin, Y., Chen, C., Han, X., Wu, B., Xu, R., Liu, W., Yan, P.*, et al.* (2016). Divergent
1019 lncRNAs Regulate Gene Expression and Lineage Differentiation in Pluripotent Cells. Cell Stem Cell *18*,
1020 637-652.

1021 Mele, M., Mattioli, K., Mallard, W., Shechner, D.M., Gerhardinger, C., and Rinn, J.L. (2017). Chromatin
1022 environment, transcriptional regulation, and splicing distinguish lincRNAs and mRNAs. Genome Res *27*,
1023 27-37.

1024 Mensah, I.K., Norvil, A.B., AlAbdi, L., McGovern, S., Petell, C.J., He, M., and Gowher, H. (2021).
1025 Misregulation of the expression and activity of DNA methyltransferases in cancer. NAR Cancer *3*,
1026 zcab045.

1027 Montgomery, K.G., Liu, M.C., Eccles, D.M., and Campbell, I.G. (2004). The DNMT3B C-->T promoter
1028 polymorphism and risk of breast cancer in a British population: a case-control study. Breast cancer
1029 research : BCR *6*, R390-394.

1030 Naumova, N., Smith, E.M., Zhan, Y., and Dekker, J. (2012). Analysis of long-range chromatin interactions
1031 using Chromosome Conformation Capture. Methods *58*, 192-203.

1032 Norvil, A.B., AlAbdi, L., Liu, B., Tu, Y.H., Forstoffer, N.E., Michie, A.R., Chen, T., and Gowher, H. (2020).
1033 The acute myeloid leukemia variant DNMT3A Arg882His is a DNMT3B-like enzyme. Nucleic Acids Res *48*,
1034 3761-3775.

1035 Okano, M., Bell, D.W., Haber, D.A., and Li, E. (1999). DNA methyltransferases Dnmt3a and Dnmt3b are
1036 essential for de novo methylation and mammalian development. Cell *99*, 247-257.

1037 Okano, M., Xie, S., and Li, E. (1998). Cloning and characterization of a family of novel mammalian DNA
1038 (cytosine-5) methyltransferases. Nature genetics *19*, 219-220.

1039 Ostler, K.R., Davis, E.M., Payne, S.L., Gosalia, B.B., Exposito-Cespedes, J., Le Beau, M.M., and Godley, L.A.
1040 (2007). Cancer cells express aberrant DNMT3B transcripts encoding truncated proteins. Oncogene *26*,
1041 5553-5563.

1042 Panda, A.C., Martindale, J.L., and Gorospe, M. (2016). Affinity Pulldown of Biotinylated RNA for
1043 Detection of Protein-RNA Complexes. Bio-protocol *6*, e2062.

1044 Pandya-Jones, A., and Black, D.L. (2009). Co-transcriptional splicing of constitutive and alternative exons.
1045 Rna *15*, 1896-1908.

1046 Peach, M., Marsh, N., Miskiewicz, E.I., and MacPhee, D.J. (2015). Solubilization of proteins: the
1047 importance of lysis buffer choice. Methods Mol Biol *1312*, 49-60.

1048 Petell, C.J., Alabdi, L., He, M., San Miguel, P., Rose, R., and Gowher, H. (2016). An epigenetic switch
1049 regulates de novo DNA methylation at a subset of pluripotency gene enhancers during embryonic stem
1050 cell differentiation. Nucleic Acids Res *44*, 7605-7617.

1051 Pintacuda, G., Wei, G., Roustan, C., Kirmizitas, B.A., Solcan, N., Cerase, A., Castello, A., Mohammed, S.,
1052 Moindrot, B., Nesterova, T.B*., et al.* (2017). hnRNPK Recruits PCGF3/5-PRC1 to the Xist RNA B-Repeat to
1053 Establish Polycomb-Mediated Chromosomal Silencing. Mol Cell *68*, 955-969.e910.

1054 Ponjavic, J., Ponting, C.P., and Lunter, G. (2007). Functionality or transcriptional noise? Evidence for
1055 selection within long noncoding RNAs. Genome Res *17*, 556-565.

1056 Preussner, M., Schreiner, S., Hung, L.H., Porstner, M., Jack, H.M., Benes, V., Ratsch, G., and Bindereif, A.
1057 (2012). HnRNP L and L-like cooperate in multiple-exon regulation of CD45 alternative splicing. Nucleic
1058 acids research *40*, 5666-5678.

1059 Rinn, J.L., Kertesz, M., Wang, J.K., Squazzo, S.L., Xu, X., Brugmann, S.A., Goodnough, L.H., Helms, J.A.,
1060 Farnham, P.J., Segal, E*., et al.* (2007). Functional demarcation of active and silent chromatin domains in
1061 human HOX loci by noncoding RNAs. Cell *129*, 1311-1323.

1062 Robertson, K.D., Keyomarsi, K., Gonzales, F.A., Velicescu, M., and Jones, P.A. (2000). Differential mRNA
1063 expression of the human DNA methyltransferases (DNMTs) 1, 3a and 3b during the G(0)/G(1) to S phase
1064 transition in normal and tumor cells. Nucleic acids research *28*, 2108-2113.

1065 Robertson, K.D., Uzvolgyi, E., Liang, G., Talmadge, C., Sumegi, J., Gonzales, F.A., and Jones, P.A. (1999).
1066 The human DNA methyltransferases (DNMTs) 1, 3a and 3b: coordinate mRNA expression in normal
1067 tissues and overexpression in tumors. Nucleic acids research *27*, 2291-2298.

1068 Ruan, X., Li, P., Cangelosi, A., Yang, L., and Cao, H. (2016). A Long Non-coding RNA, lncLGR, Regulates
1069 Hepatic Glucokinase Expression and Glycogen Storage during Fasting. Cell Rep *14*, 1867-1875.

1070 Saito, Y., Kanai, Y., Sakamoto, M., Saito, H., Ishii, H., and Hirohashi, S. (2002). Overexpression of a splice
1071 variant of DNA methyltransferase 3b, DNMT3b4, associated with DNA hypomethylation on
1072 pericentromeric satellite regions during human hepatocarcinogenesis. Proc Natl Acad Sci U S A *99*,
1073 10060-10065.

1074 Saldana-Meyer, R., Rodriguez-Hernaez, J., Escobar, T., Nishana, M., Jacome-Lopez, K., Nora, E.P.,
1075 Bruneau, B.G., Tsirigos, A., Furlan-Magaril, M., Skok, J*., et al.* (2019). RNA Interactions Are Essential for
1076 CTCF-Mediated Genome Organization. Mol Cell *76*, 412-422 e415.

1077 Schertzer, M.D., Braceros, K.C.A., Starmer, J., Cherney, R.E., Lee, D.M., Salazar, G., Justice, M., Bischoff,
1078 S.R., Cowley, D.O., Ariel, P*., et al.* (2019). lncRNA-Induced Spread of Polycomb Controlled by Genome
1079 Architecture, RNA Abundance, and CpG Island DNA. Mol Cell *75*, 523-537 e510.

1080 Seila, A.C., Calabrese, J.M., Levine, S.S., Yeo, G.W., Rahl, P.B., Flynn, R.A., Young, R.A., and Sharp, P.A.
1081 (2008). Divergent transcription from active promoters. Science *322*, 1849-1851.

1082 Shen, H., Wang, L., Spitz, M.R., Hong, W.K., Mao, L., and Wei, Q. (2002). A novel polymorphism in human
1083 cytosine DNA-methyltransferase-3B promoter is associated with an increased risk of lung cancer. Cancer
1084 research *62*, 4992-4995.

1085 Shukla, C.J., McCorkindale, A.L., Gerhardinger, C., Korthauer, K.D., Cabili, M.N., Shechner, D.M., Irizarry,
1086 R.A., Maass, P.G., and Rinn, J.L. (2018). High-throughput identification of RNA nuclear enrichment
1087 sequences. EMBO J *37*.

1088 Shuman, S. (2020). Transcriptional interference at tandem lncRNA and protein-coding genes: an
1089 emerging theme in regulation of cellular nutrient homeostasis. Nucleic acids research *48*, 8243-8254.

1090 Sigova, A.A., Mullen, A.C., Molinie, B., Gupta, S., Orlando, D.A., Guenther, M.G., Almada, A.E., Lin, C.,
1091 Sharp, P.A., Giallourakis, C.C.*, et al.* (2013). Divergent transcription of long noncoding RNA/mRNA gene
1092 pairs in embryonic stem cells. Proc Natl Acad Sci U S A *110*, 2876-2881.

1093 Singal, R., Das, P.M., Manoharan, M., Reis, I.M., and Schlesselman, J.J. (2005). Polymorphisms in the DNA
1094 methyltransferase 3b gene and prostate cancer risk. Oncology reports *14*, 569-573.

1095 Sleutels, F., Zwart, R., and Barlow, D.P. (2002). The non-coding Air RNA is required for silencing
1096 autosomal imprinted genes. Nature *415*, 810-813.

1097 Smith, S.A., Ray, D., Cook, K.B., Mallory, M.J., Hughes, T.R., and Lynch, K.W. (2013). Paralogs hnRNP L
1098 and hnRNP LL exhibit overlapping but distinct RNA binding constraints. PLoS One *8*, e80701.

1099 Statello, L., Guo, C.J., Chen, L.L., and Huarte, M. (2021). Gene regulation by long non-coding RNAs and its
1100 biological functions. Nat Rev Mol Cell Biol *22*, 96-118.

1101 Szyf, M. (2005). Therapeutic implications of DNA methylation. Future Oncol *1*, 125-135.

1102 Thakur, N., Tiwari, V.K., Thomassin, H., Pandey, R.R., Kanduri, M., Gondor, A., Grange, T., Ohlsson, R.,
1103 and Kanduri, C. (2004). An antisense RNA regulates the bidirectional silencing property of the Kcnq1
1104 imprinting control region. Molecular and cellular biology *24*, 7855-7862.

1105 Tian, B., and Manley, J.L. (2017). Alternative polyadenylation of mRNA precursors. Nat Rev Mol Cell Biol
1106 *18*, 18-30.

1107 Tosolini, M., and Jouneau, A. (2016). Acquiring Ground State Pluripotency: Switching Mouse Embryonic
1108 Stem Cells from Serum/LIF Medium to 2i/LIF Medium. Methods Mol Biol *1341*, 41-48.

1109 Tremblay, K.D., Duran, K.L., and Bartolomei, M.S. (1997). A 5' 2-kilobase-pair region of the imprinted
1110 mouse H19 gene exhibits exclusive paternal methylation throughout development. Molecular and
1111 cellular biology *17*, 4322-4329.

1112 Walton, E.L., Francastel, C., and Velasco, G. (2014). Dnmt3b Prefers Germ Line Genes and Centromeric
1113 Regions: Lessons from the ICF Syndrome and Cancer and Implications for Diseases. Biology *3*, 578-605.

1114 Wang, J., Bhutani, M., Pathak, A.K., Lang, W., Ren, H., Jelinek, J., He, R., Shen, L., Issa, J.P., and Mao, L.
1115 (2007). Delta DNMT3B variants regulate DNA methylation in a promoter-specific manner. Cancer
1116 research *67*, 10647-10652.

1117 Watanabe, D., Suetake, I., Tada, T., and Tajima, S. (2002). Stage- and cell-specific expression of Dnmt3a
1118 and Dnmt3b during embryogenesis. Mech Dev *118*, 187-190.

1119 Watanabe, Y., and Maekawa, M. (2010). Methylation of DNA in cancer. Advances in clinical chemistry
1120 *52*, 145-167.

1121 Weisenberger, D.J., Velicescu, M., Cheng, J.C., Gonzales, F.A., Liang, G., and Jones, P.A. (2004). Role of
1122 the DNA methyltransferase variant DNMT3b3 in DNA methylation. Mol Cancer Res *2*, 62-72.

1123 Wuarin, J., and Schibler, U. (1994). Physical isolation of nascent RNA chains transcribed by RNA
1124 polymerase II: evidence for cotranscriptional splicing. Mol Cell Biol *14*, 7219-7225.

1125 Xiang, J.F., Yin, Q.F., Chen, T., Zhang, Y., Zhang, X.O., Wu, Z., Zhang, S., Wang, H.B., Ge, J., Lu, X.*, et al.*
1126 (2014). Human colorectal cancer-specific CCAT1-L lncRNA regulates long-range chromatin interactions at
1127 the MYC locus. Cell Res *24*, 513-531.

1128 Xie, S., Wang, Z., Okano, M., Nogami, M., Li, Y., He, W.W., Okumura, K., and Li, E. (1999). Cloning,
1129 expression and chromosome locations of the human DNMT3 gene family. Gene *236*, 87-95.

1130 Xie, Z.H., Huang, Y.N., Chen, Z.X., Riggs, A.D., Ding, J.P., Gowher, H., Jeltsch, A., Sasaki, H., Hata, K., and
1131 Xu, G.L. (2006). Mutations in DNA methyltransferase DNMT3B in ICF syndrome affect its regulation by
1132 DNMT3L. Hum Mol Genet *15*, 1375-1385.

1133 Xu, G.L., Bestor, T.H., Bourc'his, D., Hsieh, C.L., Tommerup, N., Bugge, M., Hulten, M., Qu, X., Russo, J.J.,
1134 and Viegas-Pequignot, E. (1999). Chromosome instability and immunodeficiency syndrome caused by
1135 mutations in a DNA methyltransferase gene. Nature *402*, 187-191.

1136 Yagi, M., Kabata, M., Tanaka, A., Ukai, T., Ohta, S., Nakabayashi, K., Shimizu, M., Hata, K., Meissner, A.,
1137 Yamamoto, T.*, et al.* (2020). Identification of distinct loci for de novo DNA methylation by DNMT3A and
1138 DNMT3B during mammalian development. Nature Communications *11*, 3199.

1139 Yang, F., Deng, X., Ma, W., Berletch, J.B., Rabaia, N., Wei, G., Moore, J.M., Filippova, G.N., Xu, J., Liu, Y.*,*
1140 *et al.* (2015). The lncRNA Firre anchors the inactive X chromosome to the nucleolus by binding CTCF and
1141 maintains H3K27me3 methylation. Genome biology *16*, 52.

1142 Yin, Y., Lu, J.Y., Zhang, X., Shao, W., Xu, Y., Li, P., Hong, Y., Cui, L., Shan, G., Tian, B.*, et al.* (2020). U1
1143 snRNP regulates chromatin retention of noncoding RNAs. Nature *580*, 147-150.

1144 Ying, Q.L., Wray, J., Nichols, J., Batlle-Morera, L., Doble, B., Woodgett, J., Cohen, P., and Smith, A. (2008).
1145 The ground state of embryonic stem cell self-renewal. Nature *453*, 519-523.

1146 Yuan, W., Xie, J., Long, C., Erdjument-Bromage, H., Ding, X., Zheng, Y., Tempst, P., Chen, S., Zhu, B., and
1147 Reinberg, D. (2009). Heterogeneous nuclear ribonucleoprotein L Is a subunit of human KMT3a/Set2
1148 complex required for H3 Lys-36 trimethylation activity in vivo. The Journal of biological chemistry *284*,
1149 15701-15707.

1150 Zeng, Y., Ren, R., Kaur, G., Hardikar, S., Ying, Z., Babcock, L., Gupta, E., Zhang, X., Chen, T., and Cheng, X.
1151 (2020). The inactive Dnmt3b3 isoform preferentially enhances Dnmt3b-mediated DNA methylation.
1152 Genes Dev *34*, 1546-1558.

1153 Zuckerman, B., and Ulitsky, I. (2019). Predictive models of subcellular localization of long RNAs. RNA *25*,
1154 557-572.

1155

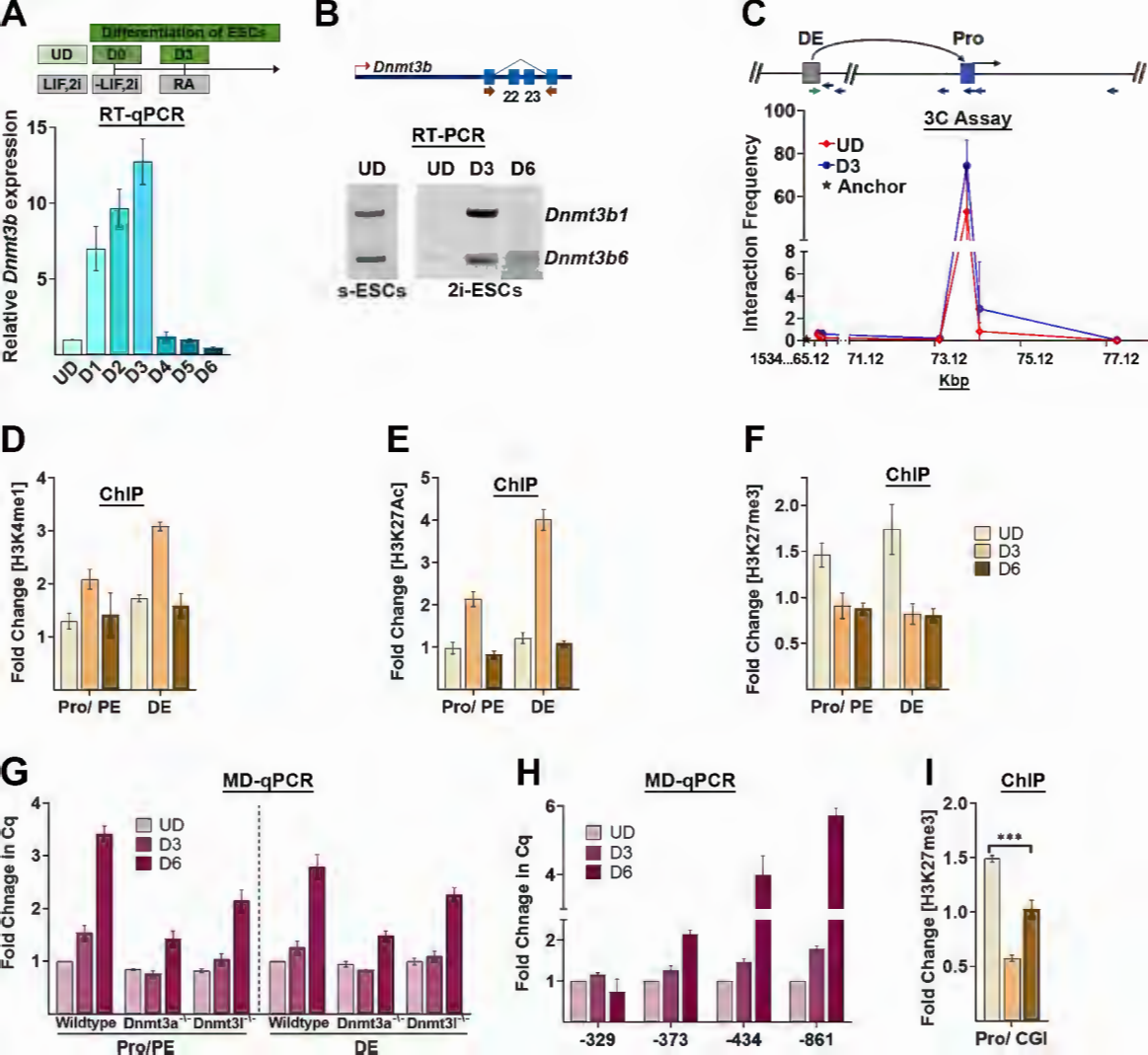
A
Differentiation of ESCs
UD
D0
D3
LIF,2i
-LIF,2i
RA
RT-qPCR
Relative Dnmt3b expression
15
10
5
UD
D1
D2
D3
D4
D5
D6
B
Dnmt3b
22 23
RT-PCR
UD
UD
D3
D6
Dnmt3b1
Dnmt3b6
s-ESCs
2i-ESCs
C
DE
Pro
3C Assay
UD
D3
Anchor
Interaction Frequency
100
80
60
8
6
4
2
0
1534...65.12
71.12
73.12
75.12
77.12
Kbp
D
ChIP
Fold Change [H3K4me1]
4
3
2
1
Pro/ PE
DE
E
ChIP
Fold Change [H3K27Ac]
5
4
3
2
1
Pro/ PE
DE
F
ChIP
Fold Change [H3K27me3]
2.0
1.5
1.0
0.5
UD
D3
D6
Pro/ PE
DE
G
MD-qPCR
Fold Chnage in Cq
4
3
2
1
UD
D3
D6
Wildtype
Dnmt3a-/-
Dnmt3l-/-
Wildtype
Dnmt3a-/-
Dnmt3l-/-
Pro/PE
DE
H
MD-qPCR
Fold Chnage in Cq
6
4
2
1
UD
D3
D6
-329
-373
-434
-861
I
ChIP
Fold Change [H3K27me3]
2.0
1.5
1.0
0.5
***
Pro/ CGI

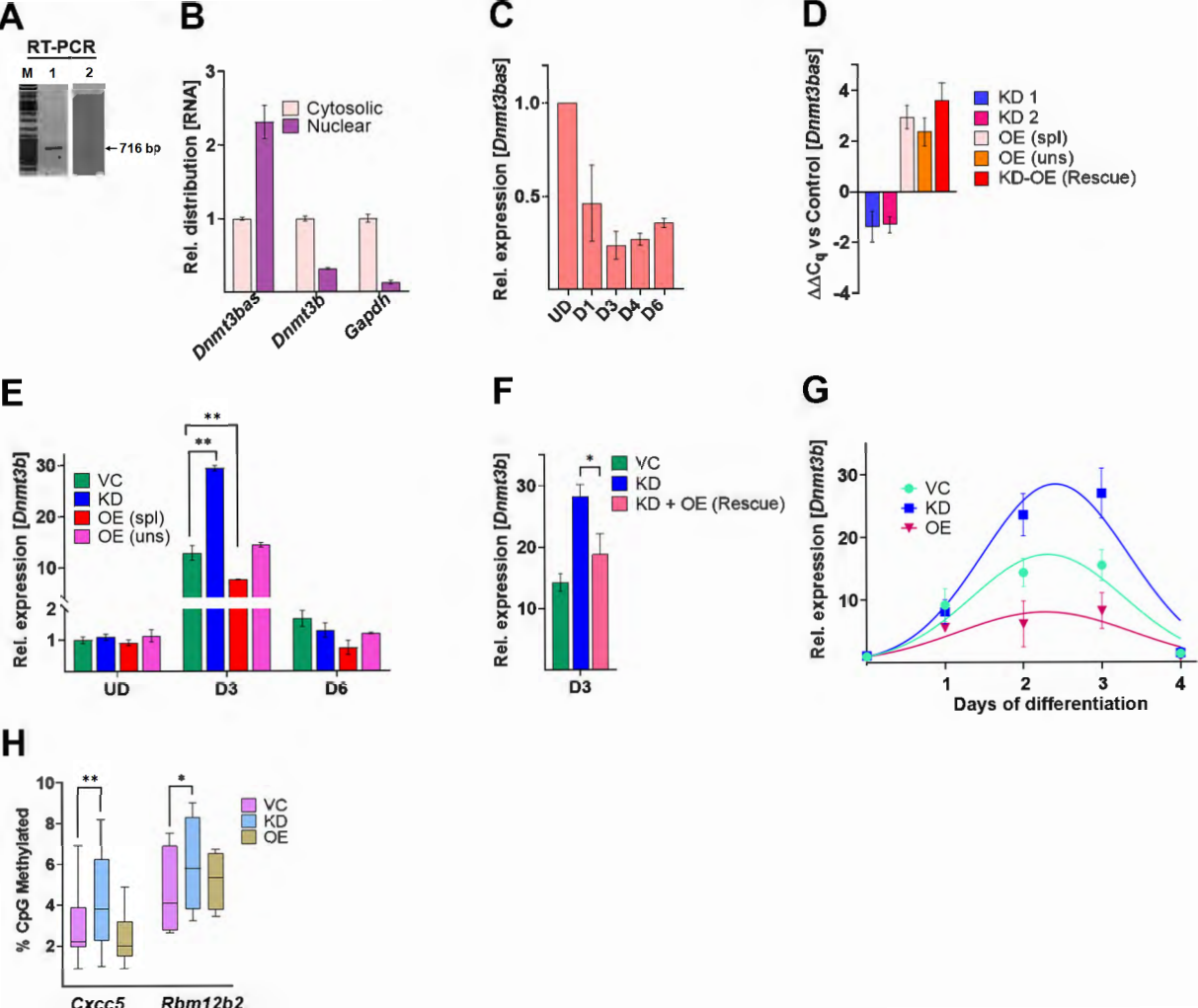
A
RT-PCR
M 1 2
716 bp
B
Rel. distribution [RNA]
Cytosolic
Nuclear
Dnmt3bas
Dnmt3b
Gapdh
C
Rel. expression [Dnmt3bas]
UD D1 D3 D4 D6
D
ΔΔCq vs Control [Dnmt3bas]
KD 1
KD 2
OE (spl)
OE (uns)
KD-OE (Rescue)
E
Rel. expression [Dnmt3b]
VC
KD
OE (spl)
OE (uns)
UD
D3
D6
F
Rel. expression [Dnmt3b]
VC
KD
KD + OE (Rescue)
D3
G
Rel. expression [Dnmt3b]
VC
KD
OE
Days of differentiation
H
% CpG Methylated
VC
KD
OE
Cxcc5
Rbm12b2

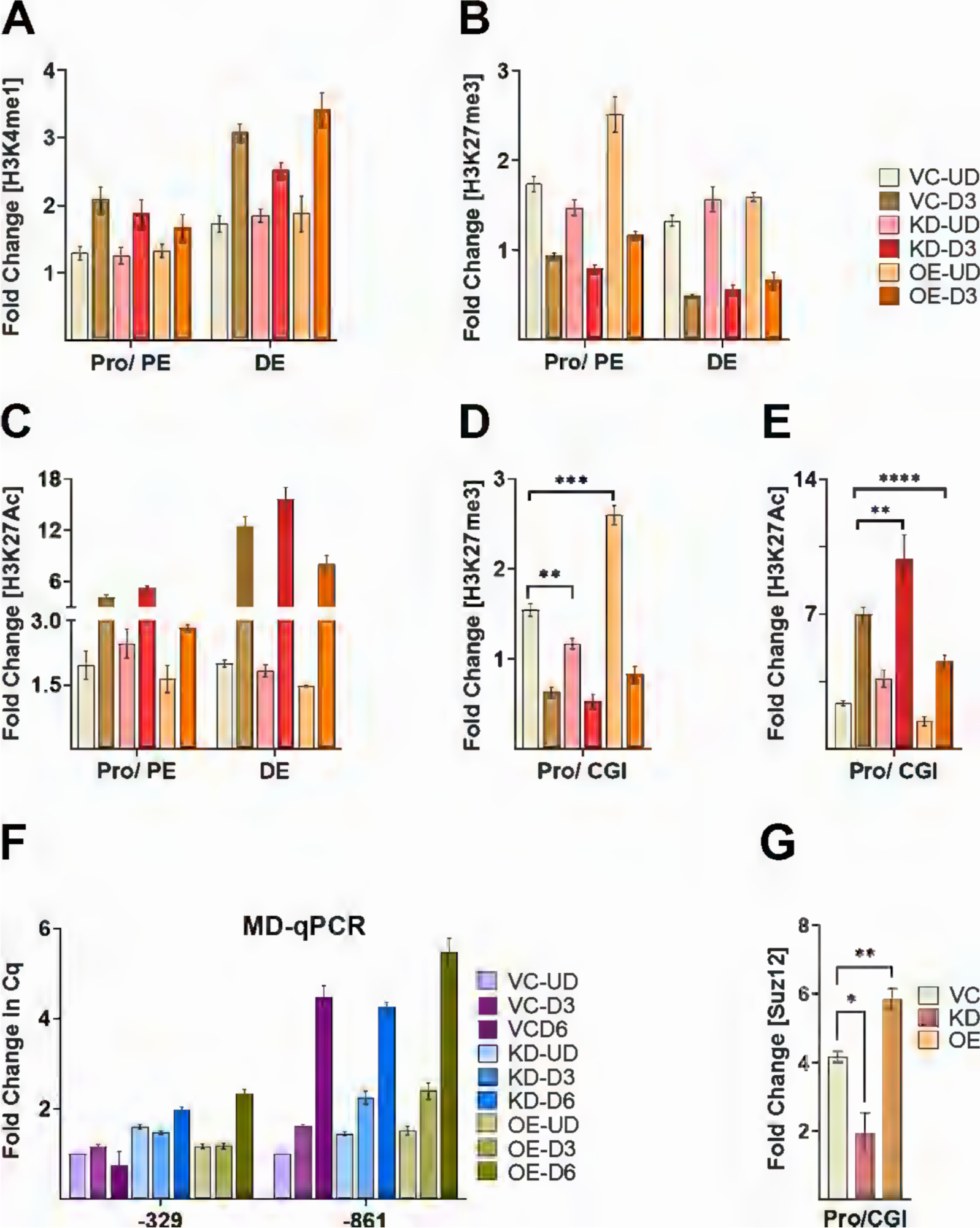
A
Fold Change [H3K4me1]
4
3
2
1
Pro/ PE
DE
B
Fold Change [H3K27me3]
3
2
1
Pro/ PE
DE
VC-UD
VC-D3
KD-UD
KD-D3
OE-UD
OE-D3
C
Fold Change [H3K27Ac]
18
12
6
3.0
1.5
Pro/ PE
DE
D
Fold Change [H3K27me3]
3
2
1
***
**
Pro/ CGI
E
Fold Change [H3K27Ac]
14
7
****
**
Pro/ CGI
F
MD-qPCR
Fold Change ln Cq
6
4
2
-329
-861
VC-UD
VC-D3
VCD6
KD-UD
KD-D3
KD-D6
OE-UD
OE-D3
OE-D6
G
Fold Change [Suz12]
8
6
4
2
**
*
Pro/CGI
VC
KD
OE

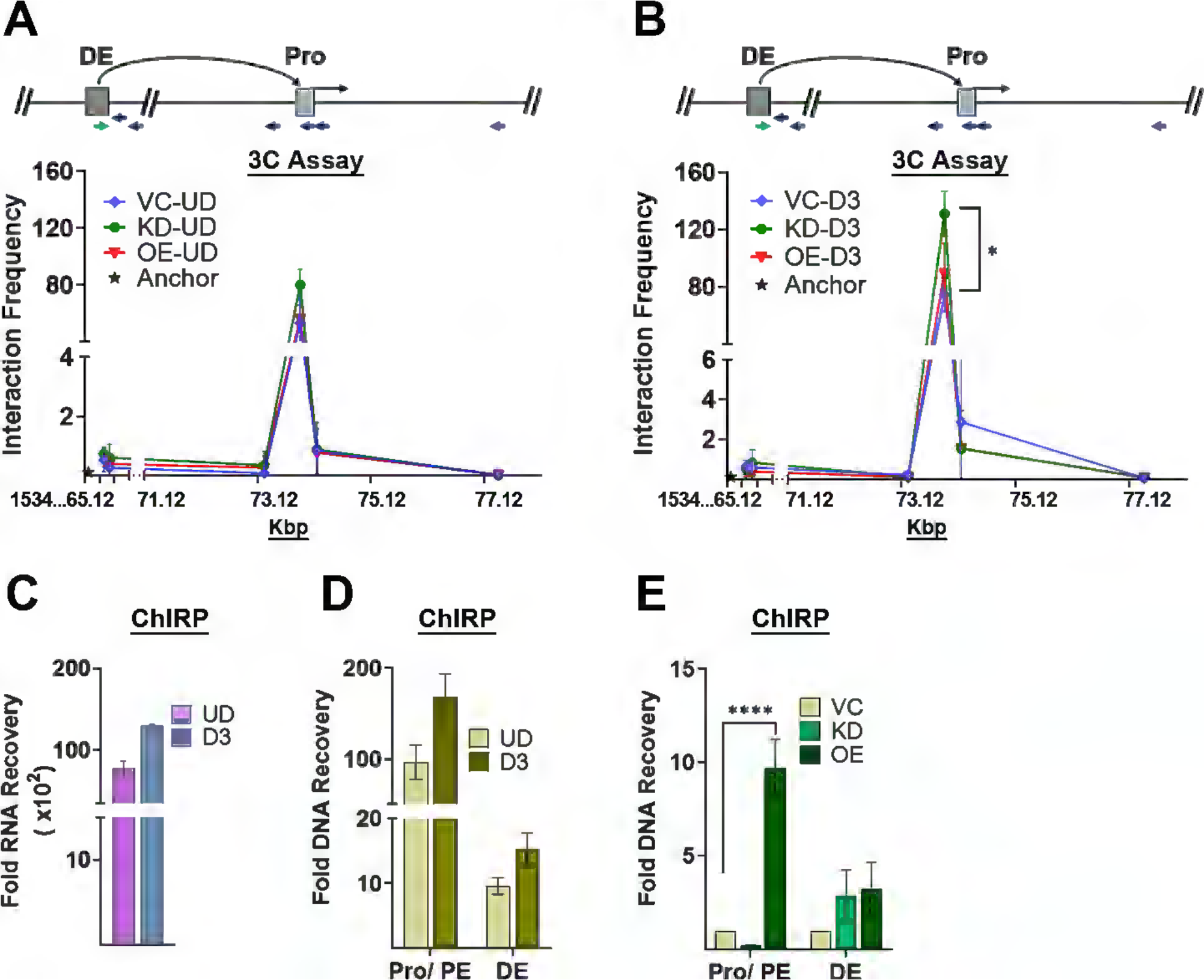
A
DE
Pro
3C Assay
Interaction Frequency
VC-UD
KD-UD
OE-UD
Anchor
160
120
80
4
2
1534...65.12
71.12
73.12
75.12
77.12
Kbp
B
DE
Pro
3C Assay
Interaction Frequency
VC-D3
KD-D3
OE-D3
Anchor
*
160
120
80
6
4
2
1534...65.12
71.12
73.12
75.12
77.12
Kbp
C
ChIRP
Fold RNA Recovery
(x10^2)
UD
D3
200
100
10
D
ChIRP
Fold DNA Recovery
UD
D3
200
100
20
10
Pro/ PE
DE
E
ChIRP
Fold DNA Recovery
****
VC
KD
OE
15
10
5
Pro/ PE
DE

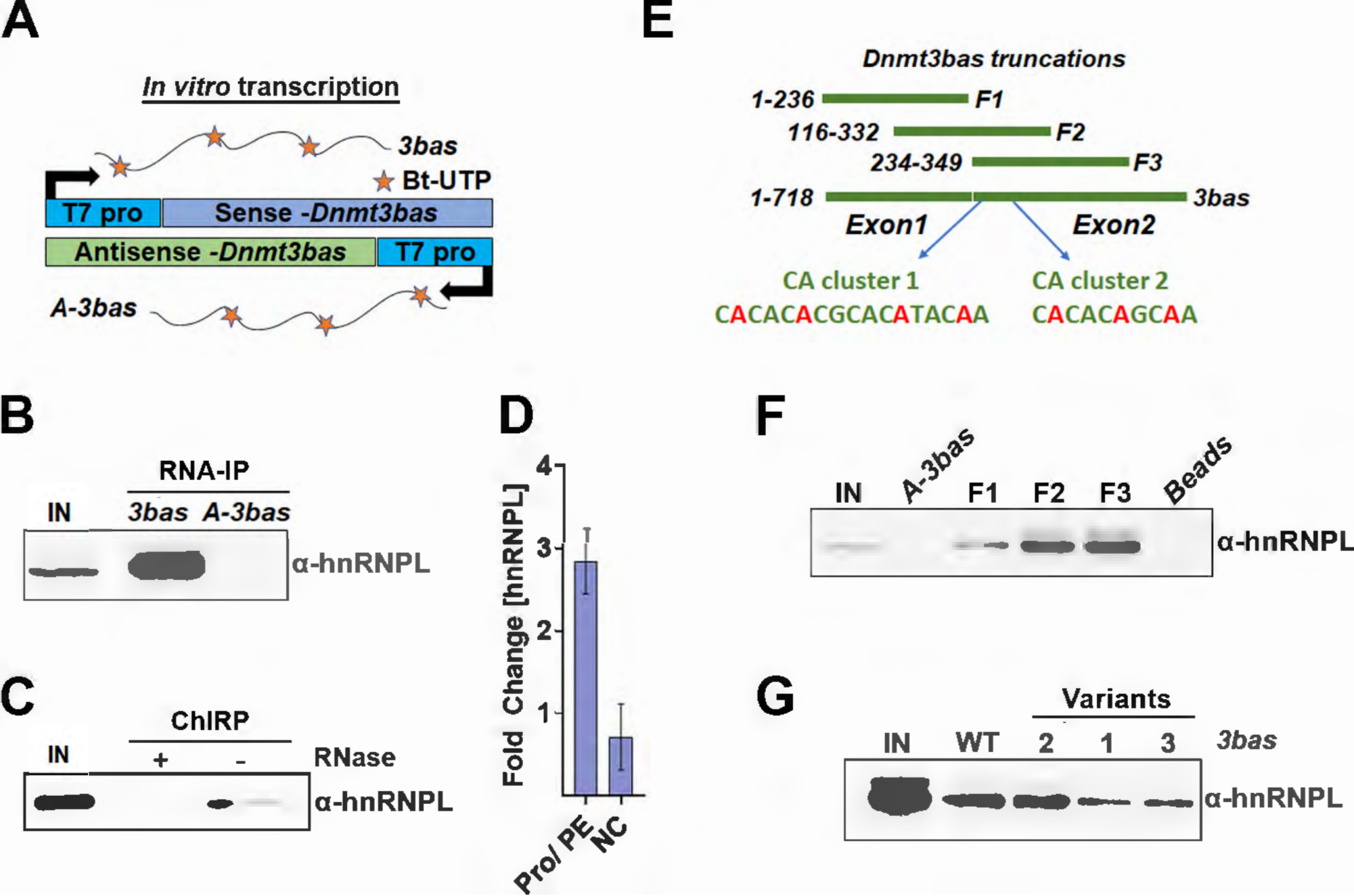
A
In vitro transcription
3bas
Bt-UTP
T7 pro
Sense -Dnmt3bas
Antisense -Dnmt3bas
T7 pro
A-3bas
E
Dnmt3bas truncations
1-236
F1
116-332
F2
234-349
F3
1-718
3bas
Exon1
Exon2
CA cluster 1
CACACACGCACATACAA
CA cluster 2
CACACAGCAA
B
RNA-IP
IN
3bas
A-3bas
α-hnRNPL
C
ChIRP
IN
+
-
RNase
α-hnRNPL
D
Fold Change [hnRNPL]
4
3
2
1
Pro/ PE
NC
F
IN
A-3bas
F1
F2
F3
Beads
α-hnRNPL
G
Variants
IN
WT
2
1
3
3bas
α-hnRNPL

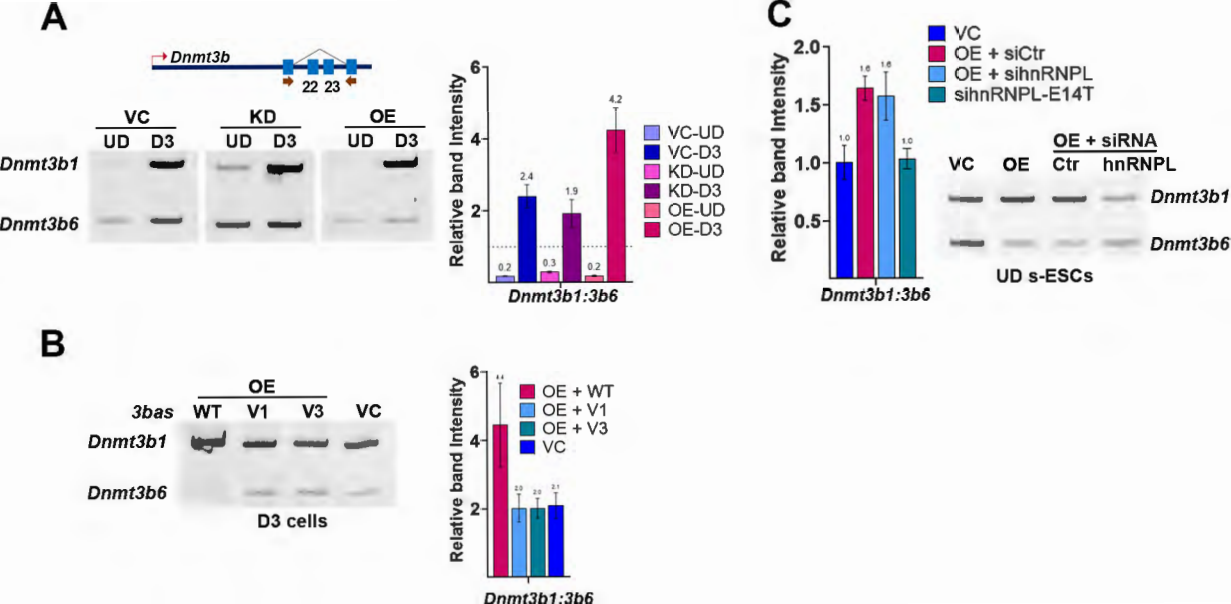
A
Dnmt3b
22 23
VC
KD
OE
UD
D3
Dnmt3b1
Dnmt3b6
Relative band Intensity
VC-UD
VC-D3
KD-UD
KD-D3
OE-UD
OE-D3
Dnmt3b1:3b6
B
OE
3bas
WT
V1
V3
VC
D3 cells
OE + WT
OE + V1
OE + V3
C
VC
OE + siCtr
OE + sihnRNPL
sihnRNPL-E14T
OE + siRNA
Ctr
hnRNPL
UD s-ESCs

Figure 7
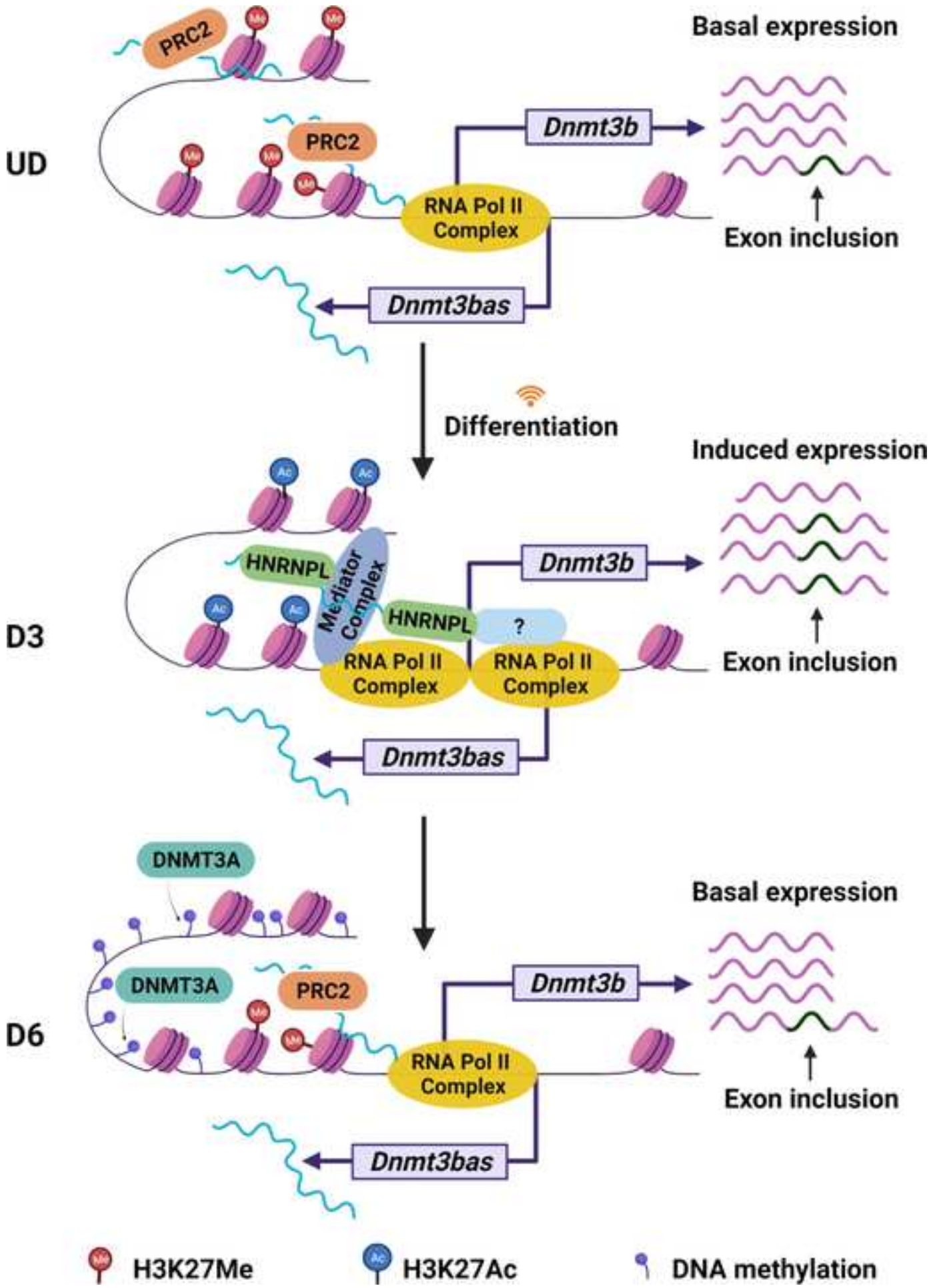
Click here to access/download;Figure;Modeltrimmed.tif